Measuring Local Proper Acceleration With Bose-Einstein Condensates

MPhil Thesis

Balázs Novák
Supervisors: Prof. Ivette Fuentes, Prof. Simone De Liberato

School of Physics and Astronomy
Faculty of Engineering and Physical Sciences
University of Southampton
Feb 2025

MPhil Thesis

Measuring Local Proper Acceleration With Bose-Einstein Condensates

by Balázs Novák

Abstract

We discuss a novel method of local absolute gravimetry using Bose-Einstein condensates, proposed in a recent patent by Ivette Fuentes et al. [1]. The calculations and early results presented there are detailed in this thesis, with a few discrepancies investigated. Furthermore, several improvements are made, which have been suggested but not carried out until now. Mainly, we employ quantum frequency interferometry as our measurement scheme, first introduced in [2], and demonstrate that it improves measurement precision by two orders of magnitude. Our semiclassical model for the system successfully accounts for certain general relativistic effects within the quantum system itself, without the need for an unrealistic, point-like reference. To do this, we adopt the methods first proposed in the patent, then developed in detail in [3]. However, we conclude that the achievable sensitivities in estimating local classical gravity is still significantly behind the performance of current best quantum technologies. We then take steps towards using our setup to measure the dynamical Casimir effect instead, as suggested in [4].

School of Physics and Astronomy
Faculty of Engineering and Physical Sciences
University of Southampton

Philosophers often think all scientists must be scientific realists. If you ask a simple question like "Are electrons real?" the answer will be "Yes". But if your questions are less superficial, for example whether some well-known scientist was a good scientist. Then, they had insisted that only empirical criteria matter and that they actually did not believe in the reality of sub-atomic entities. Ask "If that turned out to be true, would you still say they were good scientists?" The answer would reveal something about how they themselves understood what it is to be a scientist.

Bas C. Van Fraassen

Contents

Declaration of Authorship

I declare that this thesis and the work presented in it is my own and has been generated by me as the result of my own original research.

I confirm that:

1. This work was done wholly or mainly while in candidature for a research degree at this University;
2. Where any part of this thesis has previously been submitted for a degree or any other qualification at this University or any other institution, this has been clearly stated;
3. Where I have consulted the published work of others, this is always clearly attributed;
4. Where I have quoted from the work of others, the source is always given. With the exception of such quotations, this thesis is entirely my own work;
5. I have acknowledged all main sources of help;
6. Where the thesis is based on work done by myself jointly with others, I have made clear exactly what was done by others and what I have contributed myself;
7. None of this work has been published before submission

Signed:..... Date:.....

Acknowledgements

Above all, I must thank Ivette Fuentes for giving me this opportunity. Your trust allowed me to pursue my dream career today in a field that genuinely excites me. I will forever cherish the thought-provoking discussions we had in group meetings, that inspired me to become who I am.

I would also like to thank my secondary supervisor, Simone De Liberato, along with Hendrik Ulbricht and Francesco Shankar for their continued support and guidance. You truly did have my best interests at heart and this thesis might never have been written without you.

A huge thank you goes to the Philosophy of Physics community at the University of Oxford for allowing me to occasionally attend their seminar series. I met truly amazing people there and had the most fascinating discussions, broadening and enriching my research experience in physics.

I thank Hector Fernandez for all the help, patience and friendship. I could always turn to you with academic questions and expect a helping hand. I also thank Anthony Kull for his friendship. I could always trust that you would join me for a pint when no one else would. A special thanks is in order to Abdul Afzal. You introduced me to, among so many things, the world of philosophy, greatly shaping the way I see science and my interests in it. I truly hope we will continue to disagree and debate the most fascinating questions in life for many years to come.

I must express my deepest gratitude to my better half and best friend, Nina. While I say I would follow you to the end of the Earth, you actually do it. There is no end to your care and patience when it comes to supporting me and my academic career. Thank you for all your companionship, faith, solidarity, love, and not least, all the proof-reading.

Finally, I am especially thankful for my family. I feel extremely privileged by the emotional security you provide. I might not always show it, but I hope you know that I am eternally grateful.

Chapter 1

Introduction

At first glance, studying gravitational effects on quantum fields might not seem particularly propitious. The weakness of gravity compared to the other fundamental forces leads one to believe that important effects should only be expected near black holes or in the very early universe [5]. This is also what makes testing theories of quantised gravity so difficult [6].

However, the momentous advancement of quantum technologies in recent decades have yielded phenomena where general relativistic effects enter a quantum system in peculiar ways. As the scale gap between general relativity and quantum mechanics gets unprecedentedly narrow in certain cases, the need for models at the interface of the two contrasting theories has become more urgent than previously thought. For example, an atomic clock has recently demonstrated the measurement of gravitational time dilation at millimetre scales [7]. As the vapour containing the atoms is itself a comparable size, if one wishes to improve accuracies, they now need to account for the curvature of spacetime within the system of atoms itself.

In the absence of a satisfactory theory of quantum gravity, taking a semi-classical approach seems sensible. Within certain limits, one may use quantum field theory in curved spacetime to construct models that account for relativistic effects within a quantum system. In fact, this is what Maximilian Lock and his collaborators have done for the atomic clock mentioned above [8, 9].

Another fascinating example is Bose-Einstein condensates. These systems exhibit quantum properties, but due to their size also couple to gravity more strongly. For instance, it has already been investigated how oscillating gravitational fields can create excitations within these systems [10, 11]. Fur-

thermore, in a recent patent written by Ivette Fuentes et al., a novel method of measuring local gravitational acceleration using Bose-Einstein condensates was proposed with some preliminary calculations [1]. The central aim of this thesis is to complete any unfinished work of this proposal, including improvements previously suggested, and to analyse its results.

The first steps were published by Tupac Bravo, Dennis Ratzel and Ivette Fuentes in [3], where a setup with an optical oscillator was considered. It was shown how a horizontally oriented system can be used as reference for a vertically oriented one in the Schwarzschild spacetime. This not only replaces the need for an unrealistic ideal clock in the model, located infinitely far away from the Earth, but also enables us to elegantly express the gravitational time dilation inside the light clock cavity. Additionally, it was demonstrated how one could use this system to measure proper local time and local acceleration.

Following the notes in the patent and the methods developed in the paper above, we are going to extend this photonic system to Bose-Einstein condensates. The expectation is that while the optical oscillator would be better at measuring proper time, it would be greatly outperformed in measuring gravitational acceleration, due to the speed of light being replaced by the speed of sound in the condensate. Moreover, to enhance measurement sensitivities we are going to employ a novel measurement scheme introduced in [2]. Although all the calculations presented in the patent have been redone, it will be made clear what work has already been carried out previously and what has been added in this thesis. As such, references to notes in the patent will be made often.

Evidently, this project draws on several different fields in physics. We will start by introducing relativistic quantum field theory in chapter 2, where the canonical field quantisation will be set forth. Here, we will also establish the basics of quantum field theory in curved spacetime and discuss its merits and limitations. We will then review the relevant dynamics of Bose-Einstein condensates in chapter 3. At the end of this chapter, we will connect it with the previous chapter by demonstrating how one can treat these systems in a curved spacetime. To develop the measurement scheme we will be using, we present a brief introduction to Gaussian quantum metrology in chapter 4. The particular setup involving the condensate will also be introduced here. Finally, the techniques from these three chapters will be combined in chapter 5, where the central work of this thesis project is carried out. This is the only chapter containing new calculations and all previous chapters merely serve to introduce the necessary tools.

Chapter 2

Quantum Field Theory

Compatibility with Einstein's relativity has been a key consideration since the dawn of quantum mechanics [12]. When Louis de Broglie first suggested in 1923 that particles can be described using waves, one of his primary motivations was Lorentz invariance. This wave mechanics approach was then further developed by Erwin Schrödinger, who was trying to derive a relativistic wave equation. Although he was dissatisfied with his results because they initially gave the wrong fine structure for hydrogen, he realised that his non-relativistic approximation worked extremely well in a wide range of other scenarios. He published this non-relativistic wave equation, the one we now know as the *Schrödinger equation*, in a series of papers in 1926 and used it to reproduce the results of a competing approach to quantum theory (then known as matrix mechanics developed by Werner Heisenberg, Max Born, Pascual Jordan and Wolfgang Pauli in the years 1925-1926). In the position basis the equation for a free particle can be written as

$$i\hbar\frac{\partial}{\partial t}\psi(\boldsymbol{x},t)+\frac{\hbar^2}{2m}\nabla^2\psi(\boldsymbol{x},t)=0. \tag{2.1}$$

That it is not Lorentz invariant is evident from the fact that it includes a first order derivative in time but a second order derivative in space. To generalise this equation to relativistic motion one could employ the relativistic energy-momentum relation and simply square the operators, giving

$$-\hbar^2\frac{\partial^2}{\partial t^2}\psi(\boldsymbol{x},t)+\left(\hbar^2c^2\nabla^2+m^2c^4\right)\psi(\boldsymbol{x},t)=0. \tag{2.2}$$

By the time Schrödinger published the relativistic version of his wave equation it had already been independently derived by Oskar Klein and Walter

Gordon, hence it became known as the *Klein-Gordon equation*.

Despite these equations making many correct predictions, they still gave the wrong results for the fine structure. Schrödinger did realise that this was due to neglecting particle spin (specifically electron spin) in the wave equations, but it was Paul Dirac who finally derived a relativistic theory of the spinning electron in 1928. Furthermore, Dirac was also bothered by the negative probability density solutions of the Klein-Gordon equation, which he set out to resolve when deriving what we now call the *Dirac equation*. Although he succeeded in making his relativistic theory give the correct results for the fine structure, a new peculiar problem emerged. The Dirac equation predicts electrons with negative energy. Dirac became desperate to give an explanation for this, which eventually led him to propose in 1931 the existence of a new particle that has the same mass but opposite electric charge as the electron. Unaware of this prediction, Carl D. Anderson indeed discovered the positron a year later while analysing cosmic ray tracks.

Of course, today we know that there are a wide range of elementary particles, some with integer spins (bosons) and some with half-integer spins (fermions). The Dirac equation turns out to be no more general or correct than the Klein-Gordon equation, as they only differ in the class of particles they apply to; the Klein-Gordon equation to spinless bosons and the Dirac equation to fermions. They were eventually generalised to particles with arbitrary spin by Valentine Bargmann and Eugene Wigner in 1948, known as the *Bargmann–Wigner equations* [13]. As in this thesis we are working with spin-0 particles (also called scalar bosons) we are going to direct our attention to the Klein-Gordon equation.

While the Klein-Gordon equation is indeed compatible with special relativity, it is still in conflict with general relativity. The most obvious issue is that in general relativity space and time are not independent of each other; they are both components of the same 4 dimensional tensor field. In the wave equation however, space and time are not even treated on equal footings. Space appears as the eigenvalue of the position operator, but time is just there as a parameter [14]. According to standard quantum mechanics time is not a valid observable as it is not represented by a hermitian operator.

Before holding any hope to reconcile quantum mechanics with general relativity we must do one of two things. Either we promote time to be an operator as well, or we demote position to just be another parameter. For the first option, one can treat the proper time as the time parameter and promote the coordinate time to be an operator. By introducing additional parameters

this approach generalises to string theory, an active field of research today.

The other option, the one that is going to be the focus of this chapter, is demoting position. This can be done by introducing a set of new operators at each point in space and labeling them using our new parameter $\boldsymbol{x}$. The set of operators is called a *quantum field*, denoted as $\psi(\boldsymbol{x}, t)$, replacing the wave function in standard quantum mechanics (confusingly denoted the same way). This approach has been developed into what became the greatly successful standard model of particle physics.

The first field to be quantised was the electromagnetic field by Dirac in 1927 to account for spontaneous emission. His methods of using the canonical commutation relations were soon applied to other fields, specifically the wave functions of quantum mechanics. This was originally called *second quantisation*, and later *canonical quantisation*. By 1929, Heisenberg and Pauli developed a theory of general quantum fields using the Lagrangian formalism.

In this chapter we are going to quantise a scalar field using their formalism, first in flat spacetime and then discussing the generalisation to curved spacetime. To demonstrate some of the fascinating relativistic effects we are going to do this in the Rindler coordinates. For this, we start by discussing uniform proper acceleration in special relativity and using it to construct the Rindler coordinates in section 2.1. The canonical quantisation in these coordinates is then carried out in detail in section 2.2 and a quantum field theory for scalar bosons is established. Here we will also address the concern previously mentioned regarding the negative probability solutions. This explanation was originally presented by Pauli and Weisskopf in 1934 by introducing antiparticles for bosons as well. Furthermore, they demonstrated that the free field solutions behave like an infinite number of coupled harmonic oscillators. We then show in section 2.3 how the results in Rindler coordinates relate to the equivalent results in Minkowski coordinates by introducing the Bogoliubov transformations. This technique was not developed until 1958 by Nikolay Bogolyubov [15]. Finally, in section 2.4 we discuss the strengths and weaknesses of quantum field theory when applied in curved spacetimes.

2.1 Constructing the Rindler Coordinates

2.1.1 Uniform Proper Acceleration

Firstly, we define the proper acceleration in Special Relativity as the acceleration measured by an accelerometer (a device measuring acceleration locally) carried by the observer. Observers travelling with a constant proper acceleration are non-inertial and therefore have curved world-lines [16]. The Lorentz transformation can only change the usual Cartesian coordinates to inertial ones with straight world-lines. We can still use the Lorentz transformation however to change the coordinates to a specific point on a non-inertial curved world-line. This resulting set of coordinates are called a *momentarily comoving reference frame* (MCRF) [17]. At every point on the curved world-line we Lorentz transform the straight line Cartesian coordinates, with basis vectors $\vec{e}_t, \vec{e}_x$, to be tangents to the curved world-line at that point, with MCRF basis vectors $\tilde{e}_t, \tilde{e}_x$. We note that the MCRF coordinates are Minkowski orthogonal, $\tilde{e}_t \cdot \tilde{e}_x = 0$, meaning that they close equal angles with a beam of light on the spacetime diagram. We are going to work in $1+1$ dimensions, but all results can be straightforwardly generalised to $3+1$ dimensions.

It is easy to show that the two-velocity $\vec{\mathrm{U}}$, and two-acceleration $\vec{\mathrm{A}} := \frac{d\vec{\mathrm{U}}}{d\tau}$ are also Minkowski orthogonal. We begin from the fact that $\vec{\mathrm{U}} \cdot \vec{\mathrm{U}} = -c^2$ and take the proper time derivative

$$\frac{d}{d\tau}(\vec{\mathrm{U}} \cdot \vec{\mathrm{U}}) = 2(\vec{\mathrm{U}} \cdot \vec{\mathrm{A}}) = 0. \tag{2.3}$$

By definition $\vec{\mathrm{U}}$ is tangent to the curved world-line. With $\vec{\mathrm{A}}$ Minkowski orthogonal in the MCRF, $\vec{\mathrm{U}}$ must be parallel to $\tilde{e}_t$ and $\vec{\mathrm{A}}$ must be parallel to $\tilde{e}_x$. Therefore, in MCRF $\vec{\mathrm{U}}$ has only non-zero time components and $\vec{\mathrm{A}}$ has only non-zero space components. Now let us consider these two-vectors in the stationary frame and attempt to find Lorentz invariant expressions for them.

In the stationary frame we have

$$\begin{aligned}
\vec{\mathrm{U}} \cdot \vec{\mathrm{U}} &= -(\mathrm{U}^t)^2 + (\mathrm{U}^x)^2 = -c^2 \\
\vec{\mathrm{U}} \cdot \vec{\mathrm{A}} &= -\mathrm{U}^t\mathrm{A}^t + \mathrm{U}^x\mathrm{A}^x = 0 \\
\vec{\mathrm{A}} \cdot \vec{\mathrm{A}} &= -(\mathrm{A}^t)^2 + (\mathrm{A}^x)^2 = \alpha^2,
\end{aligned} \tag{2.4}$$

where α is the proper acceleration. From this set of equations through simple manipulations we can obtain the expressions

$$\mathrm{A}^{t,x} = \frac{d\mathrm{U}^{t,x}}{d\tau} = \frac{\alpha}{c}\mathrm{U}^{x,t}, \tag{2.5}$$

when the acceleration is in the positive x and t directions. We can use this to find an expression for the the second order proper time derivatives of the two-velocity components. For the spatial component, this is the differential equation:

$$\frac{d^2\mathrm{U}^x}{d\tau^2} = \frac{\alpha^2}{c^2}\mathrm{U}^x. \tag{2.6}$$

The general solutions to this equation are

$$\mathrm{U}^x(\tau) = k_1 e^{\frac{\alpha}{c}\tau} + k_2 e^{-\frac{\alpha}{c}\tau}, \tag{2.7}$$

where $k_{1,2}$ are real coefficients. We pick the convenient initial condition that $\mathrm{U}^x(0) = 0$, so that $\vec{\mathrm{U}}$ has only time components at $\tau = 0$. Therefore, we find that $k_1 = -k_2$ and thus

$$\mathrm{U}^x(\tau) = k(e^{\frac{\alpha}{c}\tau} - e^{-\frac{\alpha}{c}\tau}). \tag{2.8}$$

For the temporal component we can use equation 2.5 and get that

$$\mathrm{U}^t(\tau) = \frac{c}{\alpha}\frac{d\mathrm{U}^x}{d\tau} = k(e^{\frac{\alpha}{c}\tau} + e^{-\frac{\alpha}{c}\tau}). \tag{2.9}$$

Using again the fact that $\vec{\mathrm{U}} \cdot \vec{\mathrm{U}} = -c^2$ we can show that $-c^2 = -4k^2$. We take the sign choice in which $k = +\frac{c}{2}$, so that positive time points from past to future. We may finally write down the Lorentz invariant expressions for the two-velocity components

$$\begin{aligned} \mathrm{U}^t(\tau) &= c\cosh\frac{\alpha}{c}\tau, \\ \mathrm{U}^x(\tau) &= c\sinh\frac{\alpha}{c}\tau, \end{aligned} \tag{2.10}$$

and for the two-acceleration components

$$\begin{aligned} \mathrm{A}^t(\tau) &= \alpha\sinh\frac{\alpha}{c}\tau, \\ \mathrm{A}^x(\tau) &= \alpha\cosh\frac{\alpha}{c}\tau. \end{aligned} \tag{2.11}$$

The spacetime coordinates can be found through integrating the two-velocity components

$$\begin{aligned} ct &= \int \mathrm{U}^t d\tau = \frac{c^2}{\alpha} \sinh \frac{\alpha}{c}\tau + k_t, \\ x &= \int \mathrm{U}^x d\tau = \frac{c^2}{\alpha} \cosh \frac{\alpha}{c}\tau + k_x. \end{aligned} \tag{2.12}$$

The integration constants k_t and k_x can be set to 0 by choosing appropriate initial conditions. In this case, the spacetime interval is evaluated to be $\vec{S} \cdot \vec{S} = \left(\frac{c^2}{\alpha}\right)^2$. Therefore, the most trivial starting point for a uniformly accelerated observer on the spacetime coordinate is at $(0, \frac{c^2}{\alpha})$. The world-line can now be written down as

$$\vec{S}(\tau) = \frac{c^2}{\alpha} \sinh \left(\frac{\alpha}{c}\tau\right)\vec{e}_t + \frac{c^2}{\alpha} \cosh \left(\frac{\alpha}{c}\tau\right)\vec{e}_x, \tag{2.13}$$

which is in fact a hyperbola as expected.

We have shown how space and time are measured for an observer travelling with a constant proper acceleration. These rules can be used further to construct a new coordinate system representing the world-lines of non-inertial observers, first introduced in [18]. These coordinates are called Rindler coordinates and are discussed next.

2.1.2 Rindler Coordinates

Consider a chain of uniformly accelerating point-like particles that maintain a constant distance $D = \frac{c^2}{\alpha}$ from each other in their own reference frames. Note that a stationary observer will in fact observe the distances between the particles to be decreasing. A direct consequence of this is that each world-line in the chain must have a different proper acceleration to maintain the same proper distance between each other in their own frames. In Rindler coordinates the world-lines of these particles are used as the new coordinates [18]. We introduce the new coordinates $\frac{c^2}{\alpha} \to \chi, \tau \to \zeta$ in which we can now express the Cartesian spacetime coordinates based on equations 2.12

$$\begin{aligned} ct &= \chi \sinh \left(\frac{\alpha}{c^2}\zeta c\right), \\ x &= \chi \cosh \left(\frac{\alpha}{c^2}\zeta c\right). \end{aligned} \tag{2.14}$$

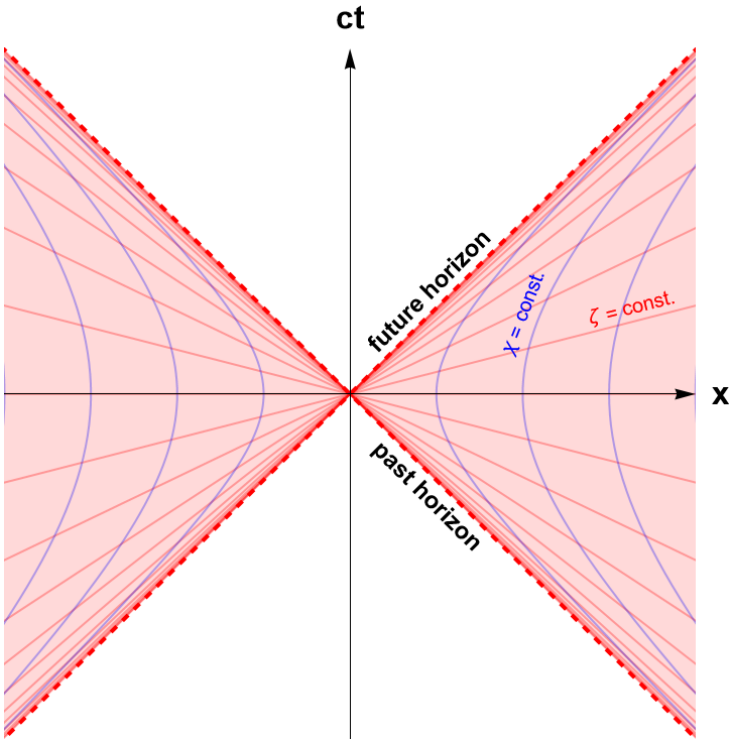

Figure 2.1: The Rindler coordinates drawn on a spacetime diagram. The pink region is called the right Rindler wedge on the positive x side and left Rindler wedge on the negative x side. The dashed red line indicates the Rindler horizon, where $\zeta = \pm\infty$.

In these new coordinates, see figure 2.1, curves of constant χ represent constant positions in MCRF and curves of constant ζ represent constant time or simultaneity in MCRF. These do not span the entire Minkowski spacetime, but just two sections of it, which are named *left and right Rindler wedges*. These sections are outlined by the *Rindler horizon*, two diagonal lines to the Cartesian coordinates crossing the origin. These lines represent the asymptotes that non-inertial world-lines are tending towards. Thus, the left and right Rindler wedges only span a quarter of the Minkowski spacetime each, as no light beam originating from outside the specific Rindler wedge can ever reach an observer travelling along one of its world-lines [19].

Note that $\tau = \zeta$ only for observers starting at $(0, D)$. Furthermore, only

these observers measure the speed of light to be c locally. In general,

$$\tau = \frac{1}{D}\chi\zeta. \tag{2.15}$$

It is also easy to show that the Rindler coordinates in terms of the Cartesian coordinates are

$$\begin{aligned} \zeta c &= \frac{c^2}{\alpha}\,\mathrm{arctanh}\,\frac{ct}{x}, \\ \chi &= \sqrt{x^2 - (ct)^2}. \end{aligned} \tag{2.16}$$

Next we will do some tensor algebraic manipulation in Rindler coordinates. Firstly, the transformation matrix Λ is identified

$$\begin{pmatrix} dt \\ dx \end{pmatrix} = \begin{pmatrix} c\chi\cosh\zeta c & \sinh\zeta c \\ c\chi\sinh\zeta c & \cosh\zeta c \end{pmatrix} \begin{pmatrix} d\zeta \\ d\chi \end{pmatrix}. \tag{2.17}$$

Now we can express the Rindler basis vectors in terms of the Cartesian ones

$$\begin{aligned} \vec{e}_\zeta &= \Lambda^x_\zeta \vec{e}_x + \Lambda^t_\zeta \vec{e}_t = c\chi\sinh(\zeta c)\vec{e}_x + c\chi\cosh(\zeta c)\vec{e}_t\,, \\ \vec{e}_\chi &= \Lambda^x_\chi \vec{e}_x + \Lambda^t_\chi \vec{e}_t = \cosh(\zeta c)\vec{e}_x + \sinh(\zeta c)\vec{e}_t\,. \end{aligned} \tag{2.18}$$

From these expressions it follows that

$$\begin{aligned} |\vec{e}_\zeta| &:= \sqrt{\vec{e}_\zeta \cdot \vec{e}_\zeta} = \sqrt{-c^2\chi^2}\,, \\ |\vec{e}_\chi| &= 1\,. \end{aligned} \tag{2.19}$$

The line element is then

$$ds^2 = -c^2dt^2 + dx^2 = -c^2\chi^2 d\zeta^2 + d\chi^2, \tag{2.20}$$

from which the Rindler metric can be read off to be

$$g_{\mu\nu} = \begin{pmatrix} -c^2\chi^2 & 0 \\ 0 & 1 \end{pmatrix}, \tag{2.21}$$

with the inverse metric

$$g^{\mu\nu} = \begin{pmatrix} -\frac{1}{c^2\chi^2} & 0 \\ 0 & 1 \end{pmatrix}. \tag{2.22}$$

Consider now a classical scalar field ϕ. As the gradient does not depend on the basis vectors we can simply express it as [16]

$$\nabla\phi := \tilde{d\phi} = \partial_\mu\phi\,\tilde{dx^\mu} = (\partial_\zeta\phi, \partial_\chi\phi)\,. \tag{2.23}$$

The tilde here denotes that the gradient is a one-form, which becomes crucial here as the equivalent vector is different in non-Cartesian coordinates. The equivalent vector in Rindler coordinates can be calculated

$$\vec{d\phi} = (g^{\zeta\zeta}\partial_\zeta\phi + g^{\zeta\chi}\partial_\chi\phi)\vec{e}_\zeta + (g^{\chi\zeta}\partial_\zeta\phi + g^{\chi\chi}\partial_\chi\phi)\vec{e}_\chi = \big(-\frac{1}{c^2\chi^2}\partial^\zeta\phi, \partial^\chi\phi\big). \quad (2.24)$$

We next calculate for the Rindler basis vectors the non-zero Christoffel symbols defined as $\Gamma^\alpha_{\beta\gamma} = (\partial_\gamma\vec{e}_\beta)^\alpha$

$$\begin{aligned} \Gamma^\chi_{\zeta\zeta} &= c\chi, \\ \Gamma^\zeta_{\chi\zeta} &= \frac{1}{c\chi}, \\ \Gamma^\zeta_{\zeta\chi} &= \frac{1}{c\chi}. \end{aligned} \quad (2.25)$$

This allows us to calculate the divergence as the contraction of $\nabla\vec{\mathrm{A}}$ for an arbitrary two-vector $\vec{\mathrm{A}}$. Note that $\nabla_\mu \mathrm{A}^\mu := \nabla\cdot\vec{\mathrm{A}}$ is frame independent. It can be evaluated using the Christoffel symbols $\nabla\cdot\vec{\mathrm{A}} = \partial_\alpha\mathrm{A}^\alpha + \Gamma^\alpha_{\mu\alpha}\mathrm{A}^\mu$. In Rindler coordinates this reads

$$\nabla\cdot\vec{\mathrm{A}} = \partial_\zeta\mathrm{A}^\zeta + \partial_\chi\mathrm{A}^\chi + \frac{1}{c\chi}\mathrm{A}^\chi = \frac{1}{c\chi}\partial_\chi(c\chi\mathrm{A}^\chi) + \partial_\zeta\mathrm{A}^\zeta. \quad (2.26)$$

Now let us substitute the vector equivalent of the field gradient from equation 2.24, $\vec{\mathrm{A}} = \vec{d\phi}$, to obtain the following expression

$$\nabla\cdot\vec{\nabla\phi} = \frac{1}{c\chi}\partial_\chi(c\chi(g^{\chi\chi}\partial_\chi\phi)) + \partial_\zeta(g^{\zeta\zeta}\partial_\zeta\phi) = \frac{1}{c\chi}\partial_\chi(c\chi(\partial^\chi\phi)) - \frac{1}{c^2\chi^2}\partial_\zeta(\partial^\zeta\phi). \quad (2.27)$$

When the divergence is 0, this is in fact the Klein-Gordon equation for a massless scalar boson in Rindler coordinates [19]. In the next section we will discuss this in much detail and quantise its solutions. There we will see that the same expression is obtained from the Lagrangian formalism, but for now we just note that this equation is consistent with the general definition of the d'Alembertian operator [5]

$$\nabla\cdot\vec{\nabla\phi} \equiv \Box\phi = \frac{1}{\sqrt{-g}}\partial_\mu(g^{\mu\nu}\sqrt{-g}\partial_\nu)\phi, \quad (2.28)$$

where $g = \det(g_{\mu\nu})$.

Another concept that is going to be important for the quantisation is Killing vector fields [5], $K = K^\mu \partial_\mu$, defined on a manifold as those satisfying the Killing equation

$$\nabla_\mu K_\nu + \nabla_\nu K_\mu = 0. \tag{2.29}$$

These describe geometrical symmetries of spacetime. For example, a time-like Killing vector field (for which $g_{\mu\nu}K^\mu K^\nu < 0$) is useful for identifying quantities that are conserved in time. For a Rindler observer this is found to be

$$K = \partial_\zeta = t\partial_x + x\partial_t. \tag{2.30}$$

Note also that the time-like property remains unchanged under any Lorentz transformation.

2.2 Canonical Field Quantisation in Rindler Coordinates

We will only consider fields defined over a smooth, connected, differentiable manifold, $\mathcal{M}$, with metric g, called spacetime. We only partially cover this manifold with the Rindler coordinates and restrict ourselves to the right Rindler wedge only. Furthermore, to simplify some of our expressions we are going to use natural units, in which $c = \hbar = 1$. We begin with the massless, non-interacting Klein-Gordon Lagrangian in flat spacetime for a classical complex field in 1+1 dimensional Rindler coordinates

$$\mathcal{L}^R_{KG} = \frac{1}{2}\sqrt{-g}g^{\mu\nu}\partial_\mu\phi(\zeta,\chi)\partial_\nu\phi^*(\zeta,\chi). \tag{2.31}$$

We take the sign convention $\eta^{\mu\nu} = diag(-1,+1)$ for the Minkowski metric. Note that ϕ and ϕ^* are treated as independent fields. Substituting in the Rindler metric from 2.22, the Lagrangian written explicitly is

$$\mathcal{L}^R_{KG} = \frac{1}{2}\big(-\frac{1}{\chi}\partial_\zeta\phi\partial^\zeta\phi^* + \chi\partial_\chi\phi\partial^\chi\phi^*\big). \tag{2.32}$$

The equations of motion obtained from the Euler-Lagrange equation are then

$$\begin{aligned}
\partial_\mu\frac{\partial\mathcal{L}^R_{KG}}{\partial\partial_\mu\phi} &= -\frac{1}{\chi}\partial_\zeta\partial^\zeta\phi^* + \partial_\chi(\chi\partial^\chi\phi^*) = 0,\\
\partial_\mu\frac{\partial\mathcal{L}^R_{KG}}{\partial\partial_\mu\phi^*} &= -\frac{1}{\chi}\partial_\zeta\partial^\zeta\phi + \partial_\chi(\chi\partial^\chi\phi) = 0.
\end{aligned} \tag{2.33}$$

These are the massless Klein-Gordon equations for ϕ and ϕ^*, equivalent to equation 2.27 in the previous section. Applying Noether's theorem we define the pseudo inner product as the conserved charge [20], which in the Rindler coordinates takes the form

$$(\phi_1, \phi_2) = -i \int_\Sigma d\chi \frac{1}{\chi} (\phi_2 \partial^\zeta \phi_1^* - \phi_1^* \partial^\zeta \phi_2), \tag{2.34}$$

where Σ is a spacelike hypersurface.

The general solutions to the Klein-Gordon equation in Rindler coordinates are of the form

$$\phi_n^R(\zeta, \chi) = N_n^R e^{i(k \ln \chi - \Omega_n \zeta)}. \tag{2.35}$$

We allow for only positive wave vectors, $k \geq 0$, and the positive sign in front of it specifies that we are working in the right Rindler wedge. We now impose boundary conditions with which we confine the field into a cavity so that $\chi_l \geq \chi \geq \chi_r$ with $0 < \chi_l < \chi_r$. The proper acceleration at the centre of the cavity is then

$$\alpha_c = \frac{2}{\chi_l + \chi_r}. \tag{2.36}$$

We also note that the edges of the cavity experience a different proper acceleration, but in their own rest frames every observer in the cavity agrees that the length of the cavity remains constant. An external stationary observer on the other hand perceives the cavity to be shrinking as it accelerates. We require the field to vanish at the boundaries, that is $\phi_n^R(\zeta, \chi_l) = \phi_n^R(\zeta, \chi_r) = 0$. Therefore, we obtain the normalised solutions of the field modes in Rindler coordinates

$$\phi_n^R(\zeta, \chi) = \frac{1}{\sqrt{\Omega_n \ln \frac{\chi_r}{\chi_l}}} \sin\left(\Omega_n \ln \frac{\chi}{\chi_l}\right) e^{-i\Omega_n \zeta}, \tag{2.37}$$

where we have defined the frequencies as $\Omega_n := +\sqrt{k^2} = n\pi / \ln \frac{\chi_r}{\chi_l}$ for mode numbers $n \in \mathbb{N}$. The full solutions to the Klein-Gordon equation are the linear combinations

$$\Phi(\zeta, \chi) = \sum_n (a_n \phi_n^R + a_n^* (\phi_n^R)^*). \tag{2.38}$$

Before we can begin the quantisation, we need to address an issue and make a distinction between the two modes, ϕ_n^R and $(\phi_n^R)^*$. Note that the

inner product of $(\phi_n^R)^*$ is negative and thus not positive definite

$$((\phi_n^R)^*, (\phi_{n'}^R)^*) = -(\phi_n^R, \phi_{n'}^R) = -\delta(n - n'). \tag{2.39}$$

Therefore, the quantised version of $\Phi(\zeta, \chi)$ cannot be interpreted as a single particle wave function. To resolve this, the solutions are split into positive and negative frequency solutions, ϕ_n^R and $(\phi_n^R)^*$ with respect to the the time-like Killing vector field via the eigenvalue equations [5, 20]

$$i\partial_\zeta \phi_n^R = +\Omega_n \phi_n^R\,, \tag{2.40}$$

$$i\partial_\zeta (\phi_n^R)^* = -\Omega_n (\phi_n^R)^*. \tag{2.41}$$

The interpretation developed by Feynman and Stückelberg is that while the positive frequency solutions describe particles, the negative frequency solutions describe negative energy particles propagating backwards in time, or equivalently positive energy antiparticles propagating forwards in time [21]. In order to quantise the field we are promoting $\Phi(\zeta, \chi)$ to be an operator-valued function by identifying a_n and a_n^* as the annihilation and creation operators respectively satisfying the commutation relation

$$[\hat{a}_n, \hat{a}_{n'}^\dagger] = \delta_{nn'}\,. \tag{2.42}$$

Thus the coefficient of the negative frequency solution is a creation operator; the operator that creates a particle as that positive energy single particle field excitation. This resolves the issue of having both positive and negative frequency solutions because our theory still only contains positive excitation energies propagating forward in time, as desired.

Operator-valued functions have well defined vacuum expectation values, but the fluctuations of the operator at a fixed point are infinite. To overcome this problem, it is common to construct a wave-packet and thereby smear the distribution over a space region. The Klein-Gordon field as a quantum operator and its momentum conjugate can now be written

$$\hat{\Phi}(\zeta, \chi) = \sum_n (\hat{a}_n \phi_n^R + \hat{a}_n^\dagger (\phi_n^R)^*), \tag{2.43}$$

$$\hat{\Pi}(\zeta, \chi) = \partial^t \hat{\Phi}(\zeta, \chi) = -i\frac{\Omega_n}{\chi} \hat{\Phi}^R(\zeta, \chi). \tag{2.44}$$

We calculate the Hamiltonian using the standard definition

$$\hat{H} = \frac{1}{2} \int d\chi \big(\hat{\Pi}^2(\zeta, \chi) + (\nabla_\chi \hat{\Phi}^R(\zeta, \chi))^2\big), \tag{2.45}$$

and the commutation relation in equation 2.42, obtaining

$$\hat{H} = \sum_n \Omega_n \left(\hat{a}_n^\dagger \hat{a}_n + \frac{1}{2}\delta(0) \right). \tag{2.46}$$

The delta function gives us an infinity in our expression for the Hamiltonian but we can get rid of it by the so-called *normal ordering*. We simply claim that we can't measure absolute energies anyway and so we are only interested in relative energies [20]. The normal ordered Hamiltonian is then written as

$$: \hat{H} := \sum_n \Omega_n \hat{a}_n^\dagger \hat{a}_n. \tag{2.47}$$

With this we are able to define the vacuum state as

$$\hat{a}_n \left|0\right\rangle = 0. \tag{2.48}$$

It is normalised as $\langle 0|0\rangle = 1$, and spans the zero particle Hilbert space denoted as $\mathbb{C}$. The single particle Hilbert space $\mathcal{H}$ is made up of the momentum eigenstates of single particles defined as

$$\left|\psi_n\right\rangle = \hat{a}_n^\dagger \left|0\right\rangle, \tag{2.49}$$

with energy eigenvalue

$$\hat{H} \left|\psi_n\right\rangle = \Omega_n \left|\psi_n\right\rangle. \tag{2.50}$$

An important prediction of Einstein's relativity is the possibility for spontaneous particle creation following the relation $E = mc^2$. To describe relativistic processes a suitable quantum theory cannot be for single particles only and a multiparticle theory is necessitated. Therefore, a single particle Hilbert space is not appropriate for a relativistic quantum field theory. Instead, we construct the Fock space by allowing for multi-particle states [5, 20]. We do this by defining the N particle Hilbert space as given by the tensor product of N single particle Hilbert spaces. The Fock space then takes the form

$$\mathbb{F} = \mathbb{C} \oplus \mathcal{H} \oplus \mathcal{H}^{\otimes 2} \oplus \mathcal{H}^{\otimes 3} \oplus ... \tag{2.51}$$

and is spanned by the states

$$\left|0\right\rangle, \hat{a}_n^\dagger \left|0\right\rangle, \hat{a}_n^\dagger \hat{a}_{n'}^\dagger \left|0\right\rangle, \hat{a}_n^\dagger \hat{a}_{n'}^\dagger \hat{a}_{n''}^\dagger \left|0\right\rangle, ... \tag{2.52}$$

Because all $\hat{a}_n^\dagger$ commute, the states are symmetric under the exchange of any two particles, eg. $|\vec{p},\vec{q}\rangle = |\vec{q},\vec{p}\rangle$. This is known as Bose-Einstein statistics, and particles with this property are called bosonic particles. Consequently, the bosonic Fock space must include this symmetrisation of the tensor products over two or more bosons

$$\mathbb{F} = \mathbb{C} \oplus \mathcal{H} \oplus \text{sym}(\mathcal{H}^{\otimes 2}) \oplus \text{sym}(\mathcal{H}^{\otimes 3}) \oplus ... \tag{2.53}$$

For example, the tensor product of two bosonic particles is symmetrised as

$$\hat{a}_n^\dagger \hat{a}_{n'}^\dagger |0\rangle = \frac{1}{\sqrt{2}} \Big(|\psi_n\rangle \otimes |\psi_{n'}\rangle + |\psi_{n'}\rangle \otimes |\psi_n\rangle \Big). \tag{2.54}$$

Throughout this thesis, only bosonic particles will be considered.

2.3 The Bogoliubov Transformation

Considering also the quantisation of the same field in Minkowski coordinates by an external stationary observer $\hat{\Phi}^M(t,x)$, we now have two equivalent sets of field equations in two different coordinates [20]. These are summarised below

$$\hat{\Phi}^M(t,x) = \sum_n (\hat{a}_n \phi_n^M + \hat{a}_n^\dagger (\phi_n^M)^*), \tag{2.55}$$

$$\hat{\Phi}^R(\zeta,\chi) = \sum_m (\hat{\bar{a}}_m \phi_m^R + \hat{\bar{a}}_m^\dagger (\phi_m^R)^*), \tag{2.56}$$

with the corresponding field modes

$$\phi_n^M(t,x) = \frac{1}{\sqrt{n\pi}} \sin\left(\omega_n (x - x_l)\right) e^{-i\omega_n t}, \tag{2.57}$$

$$\phi_m^R(\zeta,\chi) = \frac{1}{\sqrt{m\pi}} \sin\left(\Omega_m \ln \frac{\chi}{\chi_l}\right) e^{-i\Omega_m \zeta}, \tag{2.58}$$

and frequencies with $n, m \in \mathbb{N}$

$$\omega_n = \frac{n\pi}{L}, \tag{2.59}$$

$$\Omega_m = \frac{m\pi}{\ln \frac{\chi_r}{\chi_l}}. \tag{2.60}$$

There exists a transformation that allows us to change between the two representations. It is called the Bogoliubov transformation and is expressed as [5]

$$\begin{aligned}\phi_n^M(t,x) &= \sum_m \left(\alpha_{mn}^* \phi_m^R(\zeta,\chi) - \beta_{mn}\phi_m^{R*}(\zeta,\chi)\right) \\ \phi_m^R(\zeta,\chi) &= \sum_n \left(\alpha_{mn}\phi_n^M(t,x) + \beta_{mn}\phi_n^{M*}(t,x)\right)\end{aligned} \tag{2.61}$$

The Bogoliubov coefficients are defined in terms of the inner products

$$\alpha_{mn} = (\phi_m^R, \phi_n^M), \tag{2.62}$$

$$\beta_{mn} = -(\phi_m^R, \phi_n^{M*}). \tag{2.63}$$

Calculating these coefficients can be tricky, and the details for evaluating them in this particular case is presented in Appendix A. The results are

$$\begin{aligned}\alpha_{nn} =& 1 - \frac{1}{240}\pi^2 n^2 h^2 + \mathcal{O}\left(h^4\right) \qquad (n = m) \\ \alpha_{nm} =& \sqrt{mn}\frac{(-1+(-1)^{m-n})}{\pi^2(m-n)^3}h + \mathcal{O}\left(h^3\right) \qquad (n \neq m) \\ \beta_{nm} =& \sqrt{mn}\frac{(1-(-1)^{m-n})}{\pi^2(m+n)^3}h + \mathcal{O}\left(h^2\right),\end{aligned} \tag{2.64}$$

where $h := \alpha_c L/c^2$. To first order we may also express Ω_m as

$$\Omega_m = \frac{m\pi}{2\tanh^{-1}\left(\frac{h}{2}\right)} \approx \frac{L}{h}\omega_m + \mathcal{O}\left(h^2\right). \tag{2.65}$$

Furthermore, we may also write the transformation of the mode operators in the matrix form

$$\begin{bmatrix} \hat{\boldsymbol{a}} \\ \hat{\boldsymbol{a}}^\dagger \end{bmatrix} = \begin{bmatrix} \boldsymbol{\alpha}^* & -\boldsymbol{\beta}^* \\ -\boldsymbol{\beta} & \boldsymbol{\alpha} \end{bmatrix} \begin{bmatrix} \hat{\boldsymbol{a}} \\ \hat{\boldsymbol{a}}^\dagger \end{bmatrix}. \tag{2.66}$$

The transformation must be unitary, thus the coefficients have to satisfy the identities

$$\boldsymbol{\alpha}\boldsymbol{\alpha}^\dagger - \boldsymbol{\beta}\boldsymbol{\beta}^\dagger = \boldsymbol{I}, \tag{2.67}$$

$$\boldsymbol{\alpha}\boldsymbol{\beta}^\mathsf{T} = (\boldsymbol{\alpha}\boldsymbol{\beta}^\mathsf{T})^\mathsf{T}. \tag{2.68}$$

Bogoliubov transformations are therefore unitary transformations that change the basis from one set of mode solutions to another while preserving the commutation relations of the field operators.

An interesting feature of these transformations can easily be read off from equation 2.66; since β_{nm} relates creation and annihilation operators, it changes the particle content for one observer in relation to the other. In the special case when $\beta_{nm} = 0$, excitations are merely shifted between different modes. In the general case, however, what a Minkowski observer describes as vacuum, an accelerated observer will see as a populated thermal state. This is the foundation of the so-called Unruh effect [22, 23].

Change in coordinate systems is not the only example of Bogoliubov transformations. They also arise, for example, for any Gaussian operation in quantum optics, as will be shown in chapter 4. Relativistic quantum field theory therefore predicts particle creation in several, sometimes peculiar, cases. For example, particle generation during the relative motion of the boundaries confining the field is known as the *dynamical Casimir effect* [24]. This has been demonstrated experimentally first in 2011 using superconducting circuits [25].

2.4 Quantum Field Theory in Curved Spacetime

The quantisation procedure we followed in 2.2 can be straightforwardly generalised to curved spacetimes by simply allowing the background metric to be curved. The more general form of the Klein-Gordon Lagrangian density for a pseudo-Riemannian manifold is [26]

$$\mathcal{L} = \frac{1}{2}\sqrt{-g}\left(g^{\mu\nu}\partial_\mu\phi\partial_\nu\phi^* - m^2\phi^2 - \xi R\phi^2\right), \tag{2.69}$$

where ξ is a dimensionless constant and $R \equiv g^{\mu\nu}R_{\mu\nu} = g^{\mu\nu}R^{\lambda}_{\mu\lambda\nu}$ is the scalar curvature. This final term introduced represents the coupling between the scalar field and the gravitational field and has an important purpose. Recall how we removed infinities from our Hamiltonian by normal ordering in the flat spacetime case. When spacetime is curved a more elaborate procedure known as *renormalisation* is necessary [5]. The details of this procedure are outside the scope of this thesis, here we just state that in the presence of an interaction term, a new term of this form is needed for renormalisation.

The resulting Klein-Gordon equation is

$$\left(\Box + m^2 + \xi R\right)\phi = 0. \tag{2.70}$$

It can be shown that as long as the spacetime is globally hyperbolic, meaning it admits a Cauchy surface (that we used to identify the Killing vector field and hence the positive and negative frequency solutions), a unique solution exists [27].

The formulation discussed so far generalises readily to any real or complex linear bosonic field equations that are derivable from a Lagrangian and have a well posed initial value formulation, the latter of which is not trivial [27]. A formulation of quantum theory of fermion fields is also possible despite their lack of a classical limit. Its mathematical structure is closely analogous to that of the bosonic case, but with a few crucial differences. Firstly, the canonical commutation relations must be replaced by the canonical anticommutation relations. This leads to a construction based on a real inner product space rather than a real, symplectic vector space. This is compensated by taking the Hilbert space to be the anti-symmetric Fock space rather than the symmetric one discussed earlier. Finally, the generalisation to complex fermion fields has also been done with few modifications compared to the bosonic case, see for example in Dimock (1982) [28].

Does this mean we have successfully reconciled quantum theory with general relativity? Unfortunately, the answer is not yet. For example, the tension between the equivalence principle of general relativity and the superposition principle of quantum theory remains unresolved [29, 30]. In order to assign quantum properties to gravity as well, while keeping to the field theory formalism, the gravitational field itself would also need to be quantised. Sadly, gravity has proved to be nonrenormalisable with the usual perturbative methods.

Finding a suitable description for quantum gravity therefore remains to be a challenge with several different approaches actively being developed [6]. Despite its short-comings, the semiclassical framework of quantum field theory in curved spacetime (where gravity is kept classical) is still valid in a limited range of cases [5, 27]. The precise extent of this limit of validity depends on an ultimate theory of quantum gravity, therefore in its absence it is unknown. This only adds to the motivation to experimentally probe the validity of the framework in different scenarios. The expectation is that it should break down at some point as the spacetime curvature approaches the

Planck scales. Notwithstanding, the Planck length is extremely small leaving plenty of room for interesting phenomena in which the potential quantum properties of the gravitational field can be neglected and where the semiclassical theory provides an adequate description.

The semiclassical approximation even allows one to express the back-reaction effects the quantum fields bestow upon the spacetime geometry. As in general relativity, the stress-energy tensor $T_{\mu\nu}$ may be used to describe how quantum matter couples to gravity using the semiclassical Einstein equation

$$G_{\mu\nu} = 8\pi\langle T_{\mu\nu}\rangle. \tag{2.71}$$

However, expressing and calculating these expectation values turns out to be extremely difficult, especially for the physically interesting cases [27]. This limitation indeed restricts the utility of the semiclassical theory.

Nevertheless, quantum field theory in curved spacetime provides an excellent framework to study a great range of phenomena where effects from both general relativity and quantum mechanics interplay. With quantum technologies rapidly developing, reaching unprecedented measurement precision, there is an increasing number of such cases where a better theoretical understanding is crucial. For instance, the accuracy of atomic clocks are approaching the level where they would be able to resolve gravitational time dilation at scales comparable with the physical extension of the clock itself [7]. The framework of the semiclassical theory could be used to account for the curvature of spacetime within the clock. Steps in this direction were taken in [3], where the authors propose an operational way to express the clock time for a quantised light clock when it is resolving time dilation at smaller scales than its own extension. In addition, in [31] the frequency spectrum of quantised light clocks were analysed in curved spacetime for both rigid and deformable optical resonators.

Another excellent example is the exploitation of the relatively recent surge in capabilities of Bose-Einstein condensates. These systems exhibit quantum behaviour while retaining a relatively large mass, therefore coupling to gravity stronger than usual quantum systems do [32]. Quantum field theory in curved spacetime enables us to explore theoretical descriptions for scenarios harnessing this aspect of these novel technologies. For example, the possibility of using these systems to detect gravitational waves was explored in [10] and only very recently an experimental proposal was made for the extremely precise measurements of the gravitational and cosmological constants [33].

Chapter 3

Bose-Einstein Condensates

At the time of writing this, the theoretical prediction of Bose-Einstein condensation dates back exactly 100 years. In 1924 Satyendra Nath Bose published his work on the statistics of photons [34], which led Einstein to predict a peculiar phenomenon [35]: below a certain temperature threshold, a gas of massive, non-interacting bosons undergo a phase transition, with a large fraction of the particles occupying the lowest energy state. The obtained new phase is what is known as a Bose-Einstein condensate (BEC). However, the current technology at the time was far from developed for an experimental realisation. The first notable step was made by Fritz London in 1938, when he made the connection between Bose-Einstein condensation and the superfluidity of liquid ^4He [36]. The theoretical dynamics of a BEC were further developed by Bogoliubov in his 1947 theory, in which he describes elementary excitations in an interacting bosonic gas [37]. Later, in 1961, a very important result, the Gross-Pitaevskii equation was derived, describing the weakly interacting, non-uniform Bose gas in the zero temperature limit [38, 39]. In the meantime, in 1959 Eugene Hecht proposed a weakly interacting BEC made up of spin-polarized hydrogen [40]. It still took decades for the required cooling technology to be developed. It wasn't until 1995 that the first BECs were experimentally achieved by multiple groups in the same year [41, 42, 43]. They all used gases of alkali metals, namely ^{23}Na, ^{87}Rb and ^7Li, cooled using powerful laser cooling methods followed by evaporative cooling. The breakthrough finally enabled experimentation using BECs, the full potential of which is still being explored to this day.

A notable research area that sprung out of this technological breakthrough is the field of analogue models of gravity [44]. The idea to use

suitable excitations in certain matter systems that mimic the propagation of quantum fields on curved spacetime dates back to the 1980s. A well-known example is using sound waves in a moving fluid as an analogue for light propagating in a curved spacetime. It became clear in the early 2000s, hugely after the work of Luis J. Garay and collaborators [45, 46], that BECs are particularly well suited for the task. The idea is to use the so-called *acoustic metric*, first derived by William G. Unruh in the early 1980s [47], to describe an effective geometry on which acoustic disturbances travel. For instance, a group in 2010 claimed that they successfully created an analogue black hole with an event horizon from within which sound waves cannot escape [48]. The field has been vibrant in the last 25 years and developed many useful tools that can be applied outside the context of analogue gravity. In particular, we will make good use of the acoustic metric.

In this chapter, we give a very brief introduction to Bose-Einstein condensates, keeping only to the relevant points that will be necessary for our work later. As such, we will skip the usual first lesson in describing the condensation process and the ideal zero temperature example, and jump straight into the more realistic and useful case of an interacting Bose gas in section 3.1. Much of this section is based on the popular textbooks by Pethick and Smith [49] and Pitaevskii and Stringari [50]. We then go on to describe the condensate in curved spacetime and derive the aforementioned acoustic metric in section 3.2. Our approach is more closely following that of Serena Fagnocchi and his collaborators [51], but the same acoustic metric has also been derived by Matt Visser starting from a relativistic fluid dynamics description [52].

3.1 Weakly Interacting BEC

Before jumping into the microscopic theory of an interacting Bose gas, we must first make a few assumptions. Firstly, we will only be considering systems in the so-called dilute regime

$$a \ll \left(\frac{N}{V}\right)^{-1/3}, \tag{3.1}$$

where a is the s-wave scattering length, N is the total number of particles in the gas and V is the volume. For a Bose gas to condense into a BEC it has to have temperatures lower than its corresponding critical temperature $T < T_c$, which are typically of the order of nK for most alkali metals. At

these low temperatures in the dilute regime only pairwise interactions are relevant and any other scattering process can be neglected in the low-energy limit. Consequently, the scattering amplitude is completely determined by the scattering length.

In coordinate space, the effective pairwise interactions at low energies are contact interactions $\lambda\delta(\mathbf{r}-\mathbf{r}')$, with $\mathbf{r}$ and $\mathbf{r}'$ the particle positions and $\lambda = \int d\mathbf{r} U(\mathbf{r})$ for an effective potential $U(\mathbf{r})$. In momentum representation, this corresponds to just the constant $\lambda = 4\pi\hbar^2 a/m$. As we are interested in the energy of many-body states, it is convenient to apply the mean-field approximation, where all interactions are replaced by the average (effective) interaction. In a fully condensed BEC at the 0 temperature limit, all bosons occupy the single-particle state $\hat{\phi}(\mathbf{r})$. The N-particle system wave function is then

$$\hat{\Psi}(\mathbf{r}_1, \mathbf{r}_2, \ldots, \mathbf{r}_N) = \prod_{i=1}^{N} \hat{\Phi}(\mathbf{r}_i). \tag{3.2}$$

As interactions at length scales less than the interparticle spacing are neglected, the cut-off wave number can be effectively set to zero, and the effective Hamiltonian is

$$\hat{H} = \sum_{i=1}^{N} \left(\frac{\hat{\mathbf{p}}_i^2}{2m} + \hat{V}(\mathbf{r}_i) \right) + \lambda \sum_{i<j} \hat{\delta}(\mathbf{r}_i - \mathbf{r}_i). \tag{3.3}$$

Treating all atoms as being in the same state is, of course, a very idealised case and in reality a number of atoms will be in higher energy states due to the correlations at small atomic separations we have been neglecting. Particles escaping the condensate due to interactions is known as *depletion*. The order of depletion however, is less than 1% in experiments and therefore can be safely neglected.

We now introduce the wave function of the condensate itself

$$\hat{\psi}(\mathbf{r}) = \sqrt{N}\hat{\phi}(\mathbf{r}). \tag{3.4}$$

The density of particles can be written as $\rho = \left|\hat{\psi}(\mathbf{r})\right|^2$. We write the evolution

of this state in the Heisenberg picture, given by the Heisenberg equation

$$\begin{aligned} i\hbar\frac{\partial}{\partial t}\hat{\psi}(\mathbf{r},t) &= -\left[\hat{H},\hat{\psi}(\mathbf{r},t)\right] \\ &= \left(-\frac{\hbar^2}{2m}\hat{\nabla}^2 + \hat{V}(\mathbf{r},t) + \int d\mathbf{r}\hat{\psi}^\dagger(\mathbf{r}',t)U(\mathbf{r}'-\mathbf{r})\hat{\psi}(\mathbf{r}',t)\right)\hat{\psi}(\mathbf{r},t). \end{aligned} \tag{3.5}$$

From here, the Bogoliubov transformations reveal a remarkable feature of BECs.

3.1.1 Bogoliubov theory

What Bogoliubov showed in his influential work [37], was that the macroscopically occupied ground state, called the bulk of the BEC, can be treated classically, while the fluctuations around it are still described quantum mechanically. To show this, we first rewrite the Hamiltonian 3.3 in terms of the creation and annihilation operators of bosons with momentum state $\mathbf{p}$, $\hat{a}_\mathbf{p}$ and $\hat{a}^\dagger_\mathbf{p}$ respectively, which of course satisfy the usual commutation relations

$$[\hat{a}_\mathbf{p},\hat{a}^\dagger_{\mathbf{p}'}] = \delta_{\mathbf{p},\mathbf{p}'}, \qquad [\hat{a}_\mathbf{p},\hat{a}_{\mathbf{p}'}] = [\hat{a}^\dagger_\mathbf{p},\hat{a}^\dagger_{\mathbf{p}'}] = 0\,. \tag{3.6}$$

The Hamiltonian for a uniform BEC with no external potential, trapped in a box of volume V is then

$$\hat{H} = \sum_\mathbf{p}\frac{p^2}{2m}\hat{a}^\dagger_\mathbf{p}\hat{a}_\mathbf{p} + \frac{\lambda}{2V}\sum_{\mathbf{p},\mathbf{p}',\mathbf{q}}\hat{a}^\dagger_{\mathbf{p}+\mathbf{q}}\hat{a}^\dagger_{\mathbf{p}'-\mathbf{q}}\hat{a}_{\mathbf{p}'}\hat{a}_\mathbf{p}, \tag{3.7}$$

for which the solutions are plane waves

$$\hat{\psi}(\mathbf{r}) = \frac{1}{\sqrt{V}}\sum_\mathbf{p}\hat{a}_\mathbf{p}e^{\frac{i}{\hbar}\mathbf{p}\mathbf{r}}. \tag{3.8}$$

In the absence of depletion and perturbations we have

$$\hat{a}^\dagger_0\,|n\rangle = \sqrt{N+1}\,|N+1\rangle \quad \text{and} \quad \hat{a}_0\,|n\rangle = \sqrt{N}\,|N-1\rangle\,. \tag{3.9}$$

Notice that when $N \gg 1$, we can approximate $\hat{a}_0$ and $\hat{a}^\dagger_0$ by $\sqrt{N}$, known as the *Bogoliubov approximation*. This assumes that the perturbations are small, such that the number of particles that remain in the bulk, N_0, still

satisfy $N_0 \gg 1$. The total number of particles, ignoring depletion, is then given by the operator

$$\hat{N} = N_0 + \sum_{\mathbf{p}\neq 0} \hat{a}^\dagger_{\mathbf{p}} \hat{a}_{\mathbf{p}}. \tag{3.10}$$

The wave function of the ground state can thus be approximated as a classical state, ψ_0. Essentially, we are ignoring the noncommutativity of $\hat{a}_0$ and $\hat{a}^\dagger_0$ when $\left\langle \hat{a}^\dagger_0 \hat{a}_0 \right\rangle \gg 1$. This turns out to be a good approximation for describing the macroscopic phenomena associated with a BEC.

The wave function of the condensate can thus be rewritten as a classical ground state plus quantum perturbations

$$\hat{\psi}(\mathbf{r}) \approx \psi_0(\mathbf{r}) + \delta\hat{\psi}(\mathbf{r}), \tag{3.11}$$

where $\psi_0 = \sqrt{N_0}\phi_0$ and $\delta\hat{\psi} = \sum_{i\neq 0} \phi_i \hat{a}_i$. For example, the solution 3.8 then becomes

$$\hat{\psi}(\mathbf{r}) \approx \frac{1}{\sqrt{V}} \left(\sqrt{N_0} + \sum_{\mathbf{p}\neq 0} \hat{a}_{\mathbf{p}} e^{\frac{i}{\hbar}\mathbf{pr}} \right). \tag{3.12}$$

As for the Hamiltonian, it is sufficient in the Bogoliubov approximation to retain only the terms that are no more than quadratic in $\delta\hat{\psi}(\mathbf{r})$ and $\delta\hat{\psi}^\dagger(\mathbf{r})$. Therefore, one finds

$$\hat{H} = \frac{N^2\lambda}{2V} + \sum_{\mathbf{p}\neq 0} \left[\left(\frac{p^2}{2m} + \rho_0\lambda \right) \left(\hat{a}^\dagger_{\mathbf{p}} \hat{a}_{\mathbf{p}} + \hat{b}^\dagger_{\mathbf{p}} \hat{b}_{\mathbf{p}} \right) + \rho_0\lambda \left(\hat{a}^\dagger_{\mathbf{p}} \hat{b}^\dagger_{\mathbf{p}} + \hat{a}_{\mathbf{p}} \hat{b}_{\mathbf{p}} \right) \right], \tag{3.13}$$

where $\rho_0 = N_0/V$ and we introduced the operator $\hat{b}_{\mathbf{p}} := \hat{a}_{-\mathbf{p}}$. The first term gives the ground state energy of the condensate, $E_0 = \frac{1}{2}N\rho\lambda$.

We can find the eigenvalues and eigenstates of this Hamiltonian by performing the Bogoliubov transformation. We introduce two new operators defined as

$$\hat{\alpha} := u\hat{a} + v\hat{b}^\dagger, \quad \hat{\beta} := u\hat{b} + v\hat{a}^\dagger. \tag{3.14}$$

The coefficients u and v have arbitrary phases, so we choose them to be real. Due to the commutation relation properties, they must also satisfy

$$u^2 - v^2 = 1. \tag{3.15}$$

The inverse transformation gives us

$$\hat{a}_{\mathbf{p}} := u_p \hat{\alpha}_{\mathbf{p}} - v_p \hat{\alpha}^\dagger_{-\mathbf{p}}, \quad \hat{b}_{\mathbf{p}} := u_p \hat{\alpha}_{-\mathbf{p}} - v_p \hat{\alpha}^\dagger_{\mathbf{p}}. \tag{3.16}$$

The Hamiltonian can now be rewritten with only terms proportional to $\hat{\alpha}^\dagger\hat{\alpha}$

$$\hat{H} = E_0 + \frac{1}{2}\sum_{\mathbf{p}\neq 0}\left(\epsilon_p - \frac{p^2}{2m} - \rho_0\lambda\right) + \sum_{\mathbf{p}\neq 0}\left(\epsilon_p \hat{\alpha}^\dagger_{\mathbf{p}}\hat{\alpha}_{\mathbf{p}}\right). \tag{3.17}$$

Therefore, the quantum perturbations can be thought of as collective excitations creating quasi-particles and the system behaves as a collection of independent bosons with the energy spectrum

$$\epsilon_p = \sqrt{\left(\frac{p^2}{2m}\right)^2 + \frac{p^2}{m}\rho_0\lambda}. \tag{3.18}$$

The ground state is defined by the absence of excitation, i.e. $\hat{\alpha}_{\mathbf{p}}|0\rangle = 0$. In the limit of low momentum $p \ll mc_s$, where the speed of sound in the BEC is given by $c_s = \sqrt{\rho\lambda/m}$, the coefficients are of the same order $|v_{-p}| \approx |u_p|$ and the energy of the quasi-particle becomes that of a massless sound wave

$$\epsilon_p \approx pc_s. \tag{3.19}$$

For this reason, the quasi-particles are also often called phonons.

3.1.2 Time evolution

We will now have a look at the time evolution of the quasi-particles. In general, putting 3.5 and 3.11 together we get the general time-dependent *Gross-Pitaevskii* (GP) *equation*

$$i\hbar\frac{\partial}{\partial t}\hat{\psi}(\mathbf{r},t) = \left(-\frac{\hbar^2}{2m}\hat{\nabla}^2 + \hat{V}(\mathbf{r},t) + \left|\hat{\psi}(\mathbf{r},t)\right|^2\lambda\right)\hat{\psi}(\mathbf{r},t). \tag{3.20}$$

The time dependence of the ground state is simply

$$\psi_0(\mathbf{r},t) = \psi_0(\mathbf{r})e^{-\frac{i}{\hbar}\mu t}, \tag{3.21}$$

where $\mu = E(N) - E(N-1) \approx \partial E/\partial N$ is the chemical potential. For this stationary solution, the GP equation reduces to the eigenvalue equation

$$\left(-\frac{\hbar^2}{2m}\hat{\nabla}^2 + \hat{V}(\mathbf{r}) + 2\rho_0(\mathbf{r})\lambda\right)\psi_0(\mathbf{r}) = \mu\psi_0(\mathbf{r}). \tag{3.22}$$

To calculate the equations of motion for $\delta\hat{\psi}$ and $\delta\hat{\psi}^\dagger$ it is convenient to work with the operator $\hat{K} := \hat{H} - \mu\hat{N}$ rather than $\hat{H}$, since we wish to conserve particle number on average. In the Heisenberg picture the evolution is

$$i\hbar\frac{\partial}{\partial t}\delta\hat{\psi} = -\left[\hat{K}, \delta\hat{\psi}\right], \quad \text{and} \quad i\hbar\frac{\partial}{\partial t}\delta\hat{\psi}^\dagger = -\left[\hat{K}, \delta\hat{\psi}^\dagger\right]. \tag{3.23}$$

This yields the equations

$$i\hbar\frac{\partial}{\partial t}\delta\hat{\psi} = \left(-\frac{\hbar^2}{2m}\hat{\nabla}^2 + \hat{V}(\mathbf{r}) + 2\rho_0(\mathbf{r})\lambda - \mu\right)\delta\hat{\psi} + \rho_0(\mathbf{r})\lambda\delta\hat{\psi}^\dagger, \tag{3.24}$$

$$i\hbar\frac{\partial}{\partial t}\delta\hat{\psi}^\dagger = \left(-\frac{\hbar^2}{2m}\hat{\nabla}^2 + \hat{V}(\mathbf{r}) + 2\rho_0(\mathbf{r})\lambda - \mu\right)\delta\hat{\psi}^\dagger + \rho_0(\mathbf{r})\lambda\delta\hat{\psi}. \tag{3.25}$$

In the above we made use of the relation $\rho_0 = |\psi_0|^2$. We can solve these coupled equations using the Bogoliubov transformation from before, writing

$$\delta\hat{\psi}(\mathbf{r}, t) = \sum_i \left(u_i(\mathbf{r})\alpha_i e^{-\frac{i}{\hbar}\epsilon_i t} - v_i^*(\mathbf{r})\alpha_i^\dagger e^{-\frac{i}{\hbar}\epsilon_i t}\right). \tag{3.26}$$

By substitution we can see that the coefficients u_i and v_i satisfy what are called the *Bogoliubov equations*

$$\left(-\frac{\hbar^2}{2m}\hat{\nabla}^2 + \hat{V}(\mathbf{r}) + 2\rho_0(\mathbf{r})\lambda - \mu - \epsilon_i\right)u_i(\mathbf{r}) - \rho_0(\mathbf{r})\lambda v_i(\mathbf{r}) = 0, \tag{3.27}$$

$$\left(-\frac{\hbar^2}{2m}\hat{\nabla}^2 + \hat{V}(\mathbf{r}) + 2\rho_0(\mathbf{r})\lambda - \mu + \epsilon_i\right)v_i(\mathbf{r}) - \rho_0(\mathbf{r})\lambda u_i(\mathbf{r}) = 0. \tag{3.28}$$

3.1.3 Thomas-Fermi approximation

Another approximation that will be important for us is the *Thomas-Fermi approximation*. This is a common approximation made for trapped BECs, in which we assume that the the number of atoms is sufficiently large and the interactions are repulsive. The consequence is that the kinetic energy is small in comparison to the potential and interaction energies. In the Thomas-Fermi approximation, one neglects the kinetic energy term from the very start, in which case the time-independent GP equation reduces to

$$\left(\hat{V}(\mathbf{r}) + \left|\hat{\psi}(\mathbf{r})\right|^2\lambda\right)\hat{\psi}(\mathbf{r}) = \mu\hat{\psi}(\mathbf{r}). \tag{3.29}$$

This yields an important solution for $\psi_0(\mathbf{r})$, which can be expressed in the useful form

$$\rho_0 = \frac{1}{\lambda}(\mu - V(\mathbf{r})). \tag{3.30}$$

This result can be interpreted as the energy to add a particle being the same at every point in the gas.

This can be generalised in 3+1 dimensions to the eikonal approximation, which requires that all background quantities are approximately constant. This is important for BECs on a curved spacetime background, and it has the same consequence that the kinetic energy term is discarded.

3.2 BEC In Curved Spacetime

We are now ready to tackle the dynamics of BECs in curved spacetime, described by the background metric g_{ij} with determinant $\mathbf{g}$. We will start with a relativistic description but then move on to only consider atoms in the non-relativistic limit. This is more realistic for standard BEC experiments, but it also avoids having to deal with anti-bosons. We will make use of all the approximations and assumptions made in the previous section, in particular note that 3.11 still holds, but we make a slight change in the notation, writing

$$\hat{\psi} = \psi_0(1 + \hat{\varphi}). \tag{3.31}$$

We are still decomposing the field into a classical and a quantum component, but expressed this way it will be more convenient in the calculations in this section. Additionally, we adopt the Madelung representation for ψ_0 and write it in terms of its modulus and its phase $\theta(x^\mu)$

$$\psi_0 = \sqrt{\rho_0}e^{i\theta}. \tag{3.32}$$

As our starting point, consider the Lagrangian density for an interacting relativistic BEC, which can be written as

$$\hat{\mathcal{L}}(x^\sigma) = \sqrt{-\mathbf{g}}g^{ab}\partial_\mu\hat{\psi}^\dagger\partial_\nu\hat{\psi} - \left(\frac{m^2c^2}{\hbar^2} + V(x^\sigma)\right)\hat{\psi}^\dagger\hat{\psi} - \lambda(\hat{\psi}^\dagger\hat{\psi})^2. \tag{3.33}$$

The Euler-Lagrange equation for the bulk of the BEC is then found to be

$$\Box_g\psi - \left(\frac{mc^2}{\hbar} + V(x^\mu)\right)\psi - 2\rho_0\lambda = 0, \tag{3.34}$$

where $\Box_g$ is the generalised d'Alembert operator for spacetime metric g. It is easily checked that in the non-relativistic limit the corresponding GP equation 3.22 is recovered.

We now define a few useful quantities. Firstly, a quantity with dimensions of velocity, encoding the strength of the interaction

$$c_0^2 := \frac{\hbar^2}{m^2}\lambda\rho_0. \tag{3.35}$$

We introduce the four-current u^μ that can be related to the conserved Noether current

$$j_\mu \equiv \frac{1}{2i}(\psi_0\partial_\mu\psi_0^* - \psi_0^*\partial_\mu\psi_0) = \rho_0\frac{m}{\hbar}u_\mu, \tag{3.36}$$

where we define

$$u^\mu := \frac{\hbar}{m}g^{\mu\nu}\partial_\nu\theta. \tag{3.37}$$

We can write the equations of motion for the bulk 3.34 in terms of these quantities and obtain equations

$$\partial_\mu(\rho_0 u^\mu) = 0 \tag{3.38}$$

$$-u_\mu u^\mu = c^2 + \frac{\hbar^2}{m^2}\left(V(x^\mu) + 2\lambda\rho_0 - \frac{1}{\sqrt{\rho_0}}\Box_g\sqrt{\rho_0}\right). \tag{3.39}$$

The first equation is none other than the continuity equation, ensuring that the Noether current is indeed conserved. The second one can be used to find the chemical potential, $\mu \equiv mcu^0$, as a function of u^a, λ and ρ_0.

Before expressing the equation of motion of the phonon modes, let us reiterate some assumptions. Specifically, we mentioned at the end of the last section that the eikonal approximation is going to be important here. We can now spell out what this assumption entails. We require that all background quantities vary slowly in time compared to the frequency Ω of the phonon modes $\hat{\varphi}$

$$\left|\frac{\partial_t\rho}{\rho}\right| \ll \Omega\,, \quad \left|\frac{\partial_t c_0}{c_0}\right| \ll \Omega\,, \quad \left|\frac{\partial_t u_\mu}{u_\mu}\right| \ll \Omega\,, \tag{3.40}$$

and in space compared to the wavelength. Under these assumptions the kinetic energy term can be neglected in the equations of motion for the perturbations, therefore this can be thought of as the Thomas-Fermi limit. The phonons are then described simply by the massless Klein-Gordon equation

$$\Box_G\delta\hat{\psi} = 0, \tag{3.41}$$

or in terms of the quantities defined in this section

$$\left(u^\mu \partial_\mu \frac{1}{c_0^2} u^\nu \partial_\nu - \frac{1}{\rho_0} g^{\mu\nu} \partial_\mu \rho_0 \partial_\nu\right) \hat{\varphi} = 0. \tag{3.42}$$

We can rewrite this using the continuity equation 3.38 to commute $\rho_0 u^\mu$ with ∂_μ and arrive at

$$\partial_\mu \left(\frac{\rho_0}{c_0^2} u^\mu u^\nu - \rho_0 g^{\mu\nu}\right) \partial_\nu \hat{\varphi} = 0. \tag{3.43}$$

From this equation we can identify the bracketed expression as $\sqrt{-G}G^{\mu\nu}$ in the operator $\Box_G$, with the acoustic metric

$$G_{\mu\nu} = \frac{\rho_0}{\sqrt{1 - u_\sigma u^\sigma / c_0^2}} \left(g_{\mu\nu}\left(1 - \frac{u_\sigma u^\sigma}{c_0^2}\right) + \frac{u_\mu u_\mu}{c_0^2}\right), \tag{3.44}$$

and its determinant, G. To simplify this slightly, we define the scalar speed of sound in the BEC as

$$c_s^2 := \frac{c^2 c_0^2}{|u_\alpha u^\alpha| + c_0^2}. \tag{3.45}$$

Thus, we get the acoustic metric in its useful form

$$G_{\mu\nu} = \rho \frac{c}{c_s} \left(g_{\mu\nu} + \left(1 - \frac{c_s^2}{c^2}\right) \frac{u_\mu u_\nu}{|u_\mu||u_\nu|}\right). \tag{3.46}$$

In analogue gravity, this metric is often used with a flat Minkowski background metric, $g_{\mu\nu} = \eta_{\mu\nu}$, and by experimentally controlling the fluid flow velocity they are able to produce an effective metric that is of the form of various spacetime metrics of interest from general relativity. For example, in [51] Fagnocchi et. al. demonstrates how to map the acoustic metric into the $k = -1$ FRW metric. However, we are actually interested in the opposite. We will be looking at solving the Klein-Gordon equation for phonon modes using the acoustic metric with a curved background spacetime when the spatial velocity flows vanish.

Chapter 4

Gaussian Quantum Metrology

The aim of quantum metrology is to maximise precision in measurements on quantum states. Suppose we are interested in estimating a parameter ϵ that is encoded in a quantum state. These types of problems are called *continuous problems*, and usually we can assume that the dependence of the quantum state on the parameter is known [53]. An experimenter may then prepare a probe state $\hat{\rho}_0$ and send it through a channel that encodes the desired parameter, transforming $\hat{\rho}_0 \to \hat{\rho}_\epsilon$. The estimation of the parameter ϵ can then be made from the statistics of N repeated measurements on identical states $\hat{\rho}_\epsilon$. All these steps together form what is known as an *estimating channel*. Our task is then to optimise the estimating channel through finding the most appropriate probe state $\hat{\rho}_0$ and measurement scheme. Here, we will only be considering continuous problems and within that field focus on the local estimation theory. This means that the parameters we are going to be dealing with are localised around a certain approximate value.

Furthermore, we are going to focus on Gaussian states and channels in our estimating channels. These have proved to be immensely useful in experimental quantum physics due to several factors. Gaussian states are easy to prepare and handle [54], resistant to decoherence [55], they admit to crucial quantum phenomena like entanglement, therefore they can be used in protocols such as quantum teleportation [56], and not least they are kind to the theorist as they are also easy to handle mathematically.

We are first going to look at how the sensitivities achievable are bounded and define the quantum Fisher information in 4.1. Then, in 4.2 we define what we mean by Gaussian states and unitaries, and how they are useful in calculating the quantum Fisher information. In writing these sections a lot of

help came from Dominik Safranek's exceptional PhD thesis [53]. This will be followed by an application to a physical setup in 4.3, utilising the dynamics of BECs. There, I will give an outline of the interferometry scheme proposed in [2] by my supervisor and her collaborator, Richard Howl.

4.1 The Quantum Cramér–Rao Bound

Suppose a classical, parameter-dependent probability distribution $p(x|\epsilon)$ and that we would like to estimate the parameter ϵ. We start by choosing an estimator $\boldsymbol{\epsilon}(X)$ for a given sample $X = (x_1, \ldots, x_N)$ [57, 58]. We then define the mean square error of the estimator as

$$\langle \Delta \boldsymbol{\epsilon}^2(X) \rangle = \int dx_1 ... dx_N (\boldsymbol{\epsilon}(X) - \epsilon)^2 p(x_1|\epsilon) ... p(x_N|\epsilon). \tag{4.1}$$

A remarkably important result from estimation theory is the *Cramér–Rao bound* which bounds the mean-square error from below, thus providing an ultimate limit to the precision

$$\langle \Delta \boldsymbol{\epsilon}^2(X) \rangle \geq \frac{1}{MF(\epsilon)}, \tag{4.2}$$

where M is the number of measurements taken and $F(\epsilon)$ is the *Fisher information* [59]. The Fisher information is a measure that gives us the amount of information carried about ϵ by a random variable with probability distribution $p(x|\epsilon)$. Mathematically, it is defined as

$$F(\epsilon) := \int dx \frac{(\partial_\epsilon p(x|\epsilon))^2}{p(x|\epsilon)}. \tag{4.3}$$

These classical concepts have quantum versions that quantum metrology has greatly benefited from. In quantum metrology, experimental set-ups often aim to estimate a parameter ϵ and the quantum Cramér–Rao bound gives a lower bound on the possible precision of the desired parameter. Calculating the most optimal precision, one is able to analyse the actual precision achieved in the lab and compare various measurement techniques against each other. In quantum mechanics, given a density matrix $\hat{\rho}_\epsilon$, $p(x|\epsilon)$ is the probability that measurement outcome x is obtained following a measurement. We denote the quantum Cramér–Rao bound as

$$\Delta\epsilon \geq \frac{1}{\sqrt{MH(\epsilon)}}, \tag{4.4}$$

where $H(\epsilon)$ is the quantum Fisher information [59, 60]. For the expression of the quantum Fisher information we first define the *Uhlmann fidelity*, a measure of 'closeness' between quantum states $\hat{\rho}_\epsilon$ and $\hat{\rho}'_\epsilon$ [61]. It gives the probability that one state will be identified as the other in a measurement and is defined as

$$\mathcal{F}(\hat{\rho}_\epsilon, \hat{\rho}'_\epsilon) := \left(\mathrm{Tr}\left\{ \sqrt{\sqrt{\hat{\rho}_\epsilon}\hat{\rho}'_\epsilon\sqrt{\hat{\rho}_\epsilon}} \right\} \right)^2 . \tag{4.5}$$

The quantum Fisher information can be written as [53]:

$$H(\epsilon) := \lim_{d\epsilon\to 0} 8\frac{1-\sqrt{\mathcal{F}(\hat{\rho}_\epsilon, \hat{\rho}_{\epsilon+d\epsilon})}}{d\epsilon^2}. \tag{4.6}$$

The difference between the classical Fisher information and the quantum Fisher information is that while the former is a measure of how much information about ϵ can be extracted for a given choice of measurement basis, the latter gives the amount of information that is in principle extractable from the quantum state, i.e. how much information the state itself yields about ϵ. The quantum Fisher information is therefore more general and we have that $F(\epsilon) \leq H(\epsilon)$. However, the form we expressed it in above is not a very useful one for calculations. It can be recast into various other forms, but the one most useful for our purposes is done using the covariance matrix formalism for Gaussian states [62], which is going to be discussed in the next section.

Considering probe states with quantum properties can provide a serious advantage over classical states. Firstly, if we consider N identical copies of the same state with the parameter ϵ encoded, quantum mechanics allows us to measure all states at once. The quantum Fisher information then scales as $H(\epsilon) \sim N$, known as the *shot-noise limit*, which is the same as for doing all N measurements separately. However, we can do better by harnessing the powers of entanglement. If one entangles the quantum states the quantum Fisher information scales according to the *Heisenberg scaling*, $H(\epsilon) \sim N^2$. This quantum enhancement is what we will exploit as well in our work.

4.2 Gaussian States And Channels

In this section we introduce Gaussian states and Gaussian unitary channels, then use them to find an expression for the quantum Fisher information.

First, consider a finite set of basis vectors $\{|\psi_i\rangle\}$ spanning the single particle Hilbert space. The corresponding annihilation and creation operators are collected into a vector

$$\hat{\mathbf{A}} = \begin{bmatrix} \hat{a}_1 \\ \vdots \\ \hat{a}_N \\ \hat{a}_1^\dagger \\ \vdots \\ \hat{a}_N^\dagger \end{bmatrix}. \tag{4.7}$$

The commutation relations can then be expressed in matrix form

$$[\hat{A}^i, \hat{A}^{j\dagger}] = K^{ij} \Rightarrow \mathbf{K} = \begin{bmatrix} \mathbf{I}_{N\times N} & 0 \\ 0 & -\mathbf{I}_{N\times N} \end{bmatrix}, \tag{4.8}$$

where we defined the matrix $\mathbf{K}$, called the *symplectic form*.

Suppose a quantum state described by a density matrix $\hat{\rho}$. The symmetric characteristic function for this state is defined as

$$\chi(\boldsymbol{\alpha}) = \mathrm{Tr}\Big\{\hat{\rho}\hat{D}(\boldsymbol{\alpha})\Big\}, \tag{4.9}$$

where $\hat{D}(\boldsymbol{\alpha}) = \exp\Big\{\hat{\mathbf{A}}^\dagger \mathbf{K}\boldsymbol{\alpha}\Big\}$ is the *Weyl displacement operator* [63]. The quantum state $\hat{\rho}$ is called *Gaussian* if its characteristic function is of Gaussian form:

$$\chi(\boldsymbol{\alpha}) = e^{-\frac{1}{4}\boldsymbol{\alpha}^\dagger \boldsymbol{\sigma}\boldsymbol{\alpha} - i\mathbf{d}^\dagger \mathbf{K}\boldsymbol{\alpha}}. \tag{4.10}$$

Here we have introduced the displacement vector, $\mathbf{d}$, and the covariance matrix, $\boldsymbol{\sigma}$, which are the first and second statistical moments of the state respectively. They are defined as

$$d^i = \mathrm{Tr}\Big\{\hat{\rho}\hat{A}^i\Big\} \tag{4.11}$$

$$\sigma_{ij} = \mathrm{Tr}\Big\{\hat{\rho}\{\Delta\hat{A}^i, \Delta\hat{A}^{j\dagger}\}\Big\}, \tag{4.12}$$

where $\{\cdot,\cdot\}$ is the anti-commutator and $\Delta\hat{\mathbf{A}} := \hat{\mathbf{A}} - \mathbf{d}$. Note that the Gaussian state is therefore a quantum state that is entirely characterised by its first and second moments. Furthermore, the covariance matrix formalism enables us to mathematically handle these states relatively easily and elegantly.

We have now defined a Gaussian state, next we define *Gaussian unitaries*. Very simply, a Gaussian unitary is an operation that transforms a Gaussian state into another Gaussian state, i.e. $\hat{\rho}' = \hat{U}\hat{\rho}\hat{U}^\dagger$. Generally, all such operators are generated via

$$\hat{U} = e^{\frac{i}{2}\hat{\mathbf{A}}^\dagger \mathbf{W}\hat{\mathbf{A}} + \hat{\mathbf{A}}^\dagger \mathbf{K}\boldsymbol{\alpha}}, \tag{4.13}$$

where we have introduced a Hermitian matrix $\mathbf{W}$. We can also interpret this as the matrix form of the Hamiltonian, $\hat{H}$, given by

$$\hat{H} = \hat{\mathbf{A}}^\dagger \mathbf{W}\hat{\mathbf{A}}. \tag{4.14}$$

Under a Gaussian transformation the displacement vector and the covariance matrix transform as

$$\mathbf{d}' = \mathbf{S}\mathbf{d} + \boldsymbol{b} \tag{4.15}$$

$$\boldsymbol{\sigma}' = \mathbf{S}\boldsymbol{\sigma}\mathbf{S}^\dagger, \tag{4.16}$$

where $\mathbf{S}$ is called the *symplectic matrix*, which we define as

$$\mathbf{S} = e^{i\mathbf{K}\mathbf{W}}, \tag{4.17}$$

and $\boldsymbol{b}$ is defined as

$$\boldsymbol{b} = \boldsymbol{\alpha}\left(\int_0^1 e^{i\mathbf{K}\mathbf{W}t}dt\right). \tag{4.18}$$

The simplicity of these transformations is what gives this formalism its core strength.

It has to be mentioned that our definition for the displacement vector 4.11 and the covariance matrix 4.12 are not the only representation used in the literature. We will work with the complex representation as it proves to be the most convenient in calculating the quantum Fisher information. However, the real representation, in terms of position and momentum operators, provides a more intuitive picture for experimental setups and a lot of authors choose to use that instead. In appendix B we discuss the different representations and how to move between them.

4.2.1 The quantum Fisher information

We now express the quantum Fisher information in a computationally more advantageous form. The full derivation can be found in [64]. For pure Gaussian state, the quantum Fisher information is expressed in the covariance

matrix formalism as [64, 65]

$$H(\epsilon) = \frac{1}{4}\mathrm{Tr}\left[\left(\boldsymbol{\sigma}^{-1}\partial_\epsilon\boldsymbol{\sigma}\right)^2\right] + 2\partial_\epsilon \boldsymbol{d}^\dagger \boldsymbol{\sigma}^{-1}\partial_\epsilon \boldsymbol{d}. \tag{4.19}$$

Utilising the symplectic matrix $\mathbf{S}$ of a Gaussian unitary transformation we define the matrix $\mathbf{P} := \mathbf{S}^{-1}\partial_\epsilon\mathbf{S}$. It can be shown that this matrix is of the form

$$\mathbf{P} = \begin{bmatrix} \mathbf{R} & \mathbf{Q} \\ \mathbf{Q}^* & \mathbf{R}^* \end{bmatrix}. \tag{4.20}$$

This may be used to somewhat simplify the expression for the quantum Fisher information above in a computational sense, to yield

$$H(\epsilon) = 2\,\mathrm{Re}\{\mathrm{Tr}\{\mathbf{Q}\mathbf{Q}^*\}\} + 2\partial_\epsilon \mathbf{d}^\dagger \boldsymbol{\sigma}^{-1}\partial_\epsilon \mathbf{d}. \tag{4.21}$$

Calculating the second term when the covariance matrix is large can still prove difficult, but further simplifications can be made in certain situations. When we have full control over the preparation of the initial quantum state described by $\mathbf{d}_0$ and $\boldsymbol{\sigma}_0 = \mathbf{S}_0 D_0 \mathbf{S}_0^\dagger$, where D_0 is the covariance matrix of a thermal state and $\mathbf{S}_0$ is the symplectic matrix of the operations performed on the thermal state, we can write the effects of the Gaussian channel encoding ϵ according to equations 4.15 and 4.16

$$\begin{aligned} \mathbf{d}_\epsilon &= \mathbf{S}_\epsilon \mathbf{d}_0 + \boldsymbol{b}_\epsilon, \\ \boldsymbol{\sigma}_\epsilon &= \mathbf{S}_\epsilon \mathbf{S}_0 \boldsymbol{\sigma}_0 \mathbf{S}_0^\dagger \mathbf{S}_\epsilon^\dagger. \end{aligned} \tag{4.22}$$

As before, we define the matrices $\mathbf{P}_\epsilon := \mathbf{S}_\epsilon^{-1}\partial_\epsilon\mathbf{S}_\epsilon$ and $\mathbf{P} = \mathbf{S}_0^{-1}\mathbf{P}_\epsilon\mathbf{S}_0$. Using these, the second term in equation 4.21 can be rewritten as

$$2\partial_\epsilon \mathbf{d}^\dagger \boldsymbol{\sigma}^{-1}\partial_\epsilon \mathbf{d} = 2(\mathbf{P}_\epsilon \mathbf{d}_0 + \mathbf{S}_\epsilon^{-1}\partial_\epsilon \boldsymbol{b}_\epsilon)^\dagger \boldsymbol{\sigma}_0^{-1}(\mathbf{P}_\epsilon \mathbf{d}_0 + \mathbf{S}_\epsilon^{-1}\partial_\epsilon \boldsymbol{b}_\epsilon). \tag{4.23}$$

This trick greatly simplifies calculations like in [2], the results of which apply to a wide variety of practical scenarios.

4.2.2 List of Gaussian unitaries

Here we provide a list of all possible Gaussian unitary channels.

For the case when $\mathbf{W} = \mathbf{0}$, we obtain the Weyl displacement operator, which is therefore the simplest non-trivial Gaussian unitary. We define the

coherent state as a Gaussian state that is characterised solely by its displacement operator. These states are eigenfunctions of the annihilation operator, i.e. $\hat{a}\,|\alpha_n\rangle = \alpha_n\,|\alpha_n\rangle$. For each mode number n in an N mode system, the coherent state is given by

$$|\alpha_n\rangle = \hat{D}(\alpha_n)\,|0\rangle = e^{-\frac{|\alpha_n|^2}{2}} \sum_{k=0}^{\inf} \frac{\alpha_n^k}{\sqrt{k!}}\,|k\rangle\,. \tag{4.24}$$

Calculating the first and second moments from their definitions we obtain

$$\mathbf{d} = \begin{bmatrix} \boldsymbol{\alpha} \\ \boldsymbol{\alpha}^* \end{bmatrix}, \quad \boldsymbol{\sigma} = \mathbf{I}. \tag{4.25}$$

Other Gaussian states and unitaries of great importance are those obtained when $\boldsymbol{\alpha} = \mathbf{0}$. In these cases, the unitary is fully described by the Hermitian matrix $\mathbf{W}$. First, we consider one-mode states ($N = 1$) and fully parameterize the Hermitian matrix as

$$\mathbf{W} = \begin{bmatrix} -\theta & ire^{i\phi} \\ -ire^{-i\phi} & -\theta \end{bmatrix}. \tag{4.26}$$

The case when $r = 0$ is called a one-mode phase shift and the corresponding Gausian unitary and symplectic matrix take the form

$$\hat{R}(\theta) = e^{-i\theta\hat{a}^\dagger\hat{a}}, \qquad \mathbf{R}(\theta) = \begin{bmatrix} e^{-i\theta} & 0 \\ 0 & e^{i\theta} \end{bmatrix}. \tag{4.27}$$

On the other hand, when $\theta = 0$, the transformation is called one-mode squeezing at a squeezing angle ϕ. Its Gaussian unitary and symplectic matrix are

$$\hat{S}(r,\phi) = e^{-\frac{r}{2}(e^{i\phi}\hat{a}^{\dagger 2} - e^{-i\phi}\hat{a}^2)}, \qquad \mathbf{S}(r,\phi) = \begin{bmatrix} \cosh r & -e^{i\phi}\sinh r \\ -e^{-i\phi}\sinh r & \cosh r \end{bmatrix}. \tag{4.28}$$

A single-mode squeezed state is obtained by acting with this operator on the vacuum state, i.e. $|S(r,\phi)\rangle = \hat{S}(r,\phi)\,|0\rangle$.

This concludes all possible one-mode Gaussian operations. Next we look at the two-mode ($N = 2$) cases, while still assuming $\boldsymbol{\alpha} = \mathbf{0}$. Our Hermitian matrix is now parameterized as follows

$$\mathbf{W} = \begin{bmatrix} -\theta_1 & -i\theta_B e^{i\phi_B} & ir_1 e^{i\phi_1} & ise^{i\theta_s} \\ i\theta_B e^{-i\phi_B} & -\theta_2 & ise^{i\theta_s} & ir_2 e^{i\phi_2} \\ -ir_1 e^{-i\phi_1} & -ise^{-i\theta_s} & -\theta_1 & i\theta_B e^{-i\phi_B} \\ -ise^{-i\theta_s} & -ir_2 e^{-i\phi_2} & -i\theta_B e^{i\phi_B} & -\theta_2 \end{bmatrix}. \tag{4.29}$$

Parameters θ_1 and θ_2 are the angles of phase shift, just like before. Setting all parameters to zero other than θ_n we recover the single-mode phase shift operator $\hat{R}_n(\theta_n)$ for mode number k. Parameters θ_B and ϕ_B define mode-mixing at the angle ϕ_B. Setting all other parameters to 0 gives the mode-mixing operator

$$\hat{B}(\theta_B, \phi_B) = e^{\theta_B(e^{i\phi_B}\hat{a}_1^\dagger\hat{a}_2 - e^{-i\phi_B}\hat{a}_2^\dagger\hat{a}_1)}. \tag{4.30}$$

The symplectic matrix for this channel is given by

$$\mathbf{B}(\theta_B, \phi_B) = \begin{bmatrix} \cos\theta_B & e^{i\phi_B}\sin\theta_B & 0 & 0 \\ -e^{-i\phi_B}\sin\theta_B & \cos\theta_B & 0 & 0 \\ 0 & 0 & \cos\theta_B & e^{-i\phi_B}\sin\theta_B \\ 0 & 0 & -e^{i\phi_B}\sin\theta_B & \cos\theta_B \end{bmatrix}. \tag{4.31}$$

Mode-mixing at angle zero, $\phi_B = 0$, corresponds to the beam-splitter.

Parameters r_n and ϕ_n define the single-mode squeezing unitaries $\hat{S}_n(r_n, \phi_n)$ for the mode denoted with n. The two-mode squeezing channel is parameterized by s and θ_s. The Gaussian unitary for this channel is

$$\hat{S}(s, \theta_s) = e^{-s(e^{i\theta_s}\hat{a}_1^\dagger\hat{a}_2^\dagger - e^{-i\theta_s}\hat{a}_1\hat{a}_2)}, \tag{4.32}$$

with corresponding symplectic matrix

$$\mathbf{S}(s, \theta_s) = \begin{bmatrix} \cosh s & 0 & 0 & -e^{i\theta_s}\sinh s \\ 0 & \cosh s & -e^{i\theta_s}\sinh s & 0 \\ 0 & -e^{-i\theta_s}\sinh s & \cosh s & 0 \\ -e^{-i\theta_s}\sinh s & 0 & 0 & \cosh s \end{bmatrix}. \tag{4.33}$$

Acting with this channel on the vacuum state, the two-mode squeezed state is obtained, $|S_T(s, \theta_s)\rangle = \hat{S}_T(s, \theta_s)\,|0\rangle$.

It turns out that these are all the possible Gaussian unitaries for all modes. This means that all multi-mode ($N > 1$) Gaussian unitaries with $\boldsymbol{\alpha} = \mathbf{0}$, are made up of just the phase-changing, mode-mixing and single- and two-mode squeezing channels and their combinations.

4.3 Application To BECs

We now turn to applications and demonstrate how these techniques may be applied to phonon modes in a BEC. The physical setup we are going to

consider was named *quantum frequency interferometry* [2]. Unlike in spatial interferometry, where waves travel along two spatially distinct paths, we will use interference between phonons created in a BEC. This way, we may increase precision without having to drastically scale up the experiment by building longer interferometer arms. Another advantage gained by this is that we can estimate parameters encoded by global unitary channels, since the modes can interact at all times.

Let us start by recalling the Hamiltonian from section 3.1.

$$\hat{H} = \int d\mathbf{r}\hat{\psi}^\dagger \left(-\frac{\hbar^2}{2m}\nabla^2 + V(\mathbf{r})\right)\hat{\psi} + \frac{\lambda}{2}\int d\mathbf{r}\hat{\psi}^\dagger\hat{\psi}^\dagger\hat{\psi}\hat{\psi}. \tag{4.34}$$

All assumptions made in that section are carried over, together with the Bogoliubov approximation, so we decompose the field operator $\hat{\psi}$ into a classical field, $\psi_0 = \sqrt{N_0}\phi_0$, representing the bulk of the BEC, and quantum fields, $\delta\hat{\psi}$, describing phonon modes. Using the Bogoliubov approximation, $\delta\hat{\psi}$ can be expressed as 3.26 and they obey the Bogoliubov equations 3.27 with the only difference being, that here we will denote ϵ_i as Ω_n.

We now take a small time-dependent potential $\gamma V_\gamma(\mathbf{r}, t)$, with $\gamma \ll 1$. This introduces an interaction term in the Hamiltonian, which can be written as

$$\begin{aligned}
\hat{H}_I(t) = \gamma \int d\mathbf{r} V_\gamma(\mathbf{r}, t)\Big[& N_0|\phi_0|^2 \\
& + \sqrt{N_0}\sum_n \left(\hat{a}_n e^{-i\vartheta(\mathbf{r})}e^{-i\Omega_n t} + \hat{a}_n^\dagger e^{i\vartheta(\mathbf{r})}e^{i\Omega_n t}\right) && (4.35) \\
& + \sum_{n,m}\big(u_n^*(\mathbf{r})u_m(\mathbf{r})\hat{a}_n^\dagger\hat{a}_m e^{i(\Omega_m-\Omega_n)t} && (4.36) \\
& \quad + \sum_{n,m} v_n(\mathbf{r})v_m^*(\mathbf{r})\hat{a}_n\hat{a}_m^\dagger e^{-i(\Omega_m-\Omega_n)t}\big) \\
& + \sum_{n,m}\big(u_n^*(\mathbf{r})v_m^*(\mathbf{r})\hat{a}_n^\dagger\hat{a}_m^\dagger e^{i(\Omega_m+\Omega_n)t} && (4.37) \\
& \quad + \sum_{n,m} u_n(\mathbf{r})v_m(\mathbf{r})\hat{a}_n\hat{a}_m e^{-i(\Omega_m+\Omega_n)t}\big)\Big],
\end{aligned}$$

where $\exp\{i\vartheta(\mathbf{r})\} := \phi_0(\mathbf{r})u_n^*(\mathbf{r}) + \phi_0^*(\mathbf{r})v_n^*(\mathbf{r})$. Just by changing the external potential $V_\gamma(\mathbf{r}, t)$, the experimenter is able to implement Gaussian unitary channels. For instance, choosing $V_\gamma(\mathbf{r}, t) = V_0 \sin \mathbf{\Omega}_+ t$ with V_0 a constant

amplitude and $\mathbf{\Omega}_{\pm} := \Omega_n \pm \Omega_m$, the term 4.37 gives the form of a two-mode squeezed state Hamiltonian

$$\hat{H}_{sq} = s\left(e^{i\theta_s}\hat{a}_n^{\dagger}\hat{a}_m^{\dagger} + e^{-i\theta_s}\hat{a}_n\hat{a}_m\right), \tag{4.38}$$

where s is the squeezing parameter and θ_s is the squeezing phase.

Another unitary that will be of use here is a three-mode mixing channel called the *tritter*. It is generated by the Hamiltonian

$$\hat{H}_{tr} = \frac{\hbar\theta_t}{\sqrt{2}}|a_0|\left[e^{i\vartheta_t}(\hat{a}_n + \hat{a}_m) + e^{-i\vartheta_t}(\hat{\alpha}_n^{\dagger} + \hat{\alpha}_m^{\dagger})\right]. \tag{4.39}$$

This channel mixes the two side modes with the bulk of the BEC $|a_0| = \sqrt{N_0}$, and can be obtained from 4.35 by choosing $V_{\gamma}(\mathbf{r}, t) = V_0 \cos(\mathbf{\Omega}_+ t)\cos(\mathbf{\Omega}_- t)$ and assuming $\vartheta_n(\mathbf{r}) \approx \vartheta_m(\mathbf{r})$.

We are now ready to build the interferometry scheme. Suppose a BEC that is initially unperturbed, so all particles are in the ground state, assumed to be a coherent state. This state will play the role of a pump beam, hence we will refer to it as the pump mode. We will consider three modes in total, with the pump mode and two phonon modes, so the initial displacement vector and covariance matrix of this system is

$$\boldsymbol{d_0} = \sqrt{N_0}\begin{bmatrix} e^{i\theta_0} \\ 0 \\ 0 \\ e^{-i\theta_0} \\ 0 \\ 0 \end{bmatrix}, \quad \boldsymbol{\sigma_0} = \mathbf{I}_{6\times 6}. \tag{4.40}$$

The phonons are then created by implementing a two-mode squeezing channel, that parametrically populates the side modes. The corresponding symplectic matrix is

$$\mathbf{S}_s = \begin{pmatrix} 1 & 0 & 0 & 0 & 0 & 0 \\ 0 & \cosh(s) & 0 & 0 & 0 & \sinh(s)e^{i\theta_s} \\ 0 & 0 & \cosh(s) & 0 & \sinh(s)e^{i\theta_s} & 0 \\ 0 & 0 & 0 & 1 & 0 & 0 \\ 0 & 0 & \sinh(s)e^{-i\theta_s} & 0 & \cosh(s) & 0 \\ 0 & \sinh(s)e^{-i\theta_s} & 0 & 0 & 0 & \cosh(s) \end{pmatrix}. \tag{4.41}$$

We assume that the pump remains undepleted and stays in a coherent state throughout these transformations. Particle number is conserved, and the number of phonons created is given by $N_p = 2\sinh^2 s$. Following this, the tritter is implemented, mixing the side modes with the pump, which will have the effect of increasing precision. The symplectic matrix for this channel is

$$\mathbf{S}_{tr} = \begin{pmatrix} \mathbf{S}_{tr,\alpha} & \mathbf{0} \\ \mathbf{0} & \mathbf{S}^*_{tr,\alpha} \end{pmatrix}, \tag{4.42}$$

where

$$\mathbf{S}_{tr,\alpha} = \begin{pmatrix} \cos(\theta_t) & \frac{-ie^{i\vartheta_t}\sin(\theta_t)}{\sqrt{2}} & \frac{-ie^{i\vartheta_t}\sin(\theta_t)}{\sqrt{2}} \\ \frac{-ie^{-i\vartheta_t}\sin(\theta_t)}{\sqrt{2}} & \cos^2\left(\frac{\theta_t}{2}\right) & -\sin^2\left(\frac{\theta_t}{2}\right) \\ \frac{-ie^{-i\vartheta_t}\sin(\theta_t)}{\sqrt{2}} & -\sin^2\left(\frac{\theta_t}{2}\right) & \cos^2\left(\frac{\theta_t}{2}\right) \end{pmatrix}. \tag{4.43}$$

We may now apply the channel that encodes the parameter ϵ we would like to estimate. This could be any convenient Gaussian channel for our purposes, like a phase-shift channel, another two-mode squeezing channel, or some mode-mixing channel. For example, in [2] it was considered how gravitational waves may implement a squeezing channel, leaving a trace through an encoded parameter. Following the encoding procedure, the 'beams are recombined', so to speak, by a reverse tritter operation followed by an active beam splitter, the reverse of the squeezing unitary. Finally, the frequency modes of the phonons are measured through a number-sum measurement. The full interferometry scheme is illustrated in figure 4.1.

The quantum Fisher information and therefore the sensitivities can then be computed using the results in 4.2.1. Multiple examples are presented in [2], but we will look at a specific case in the next chapter.

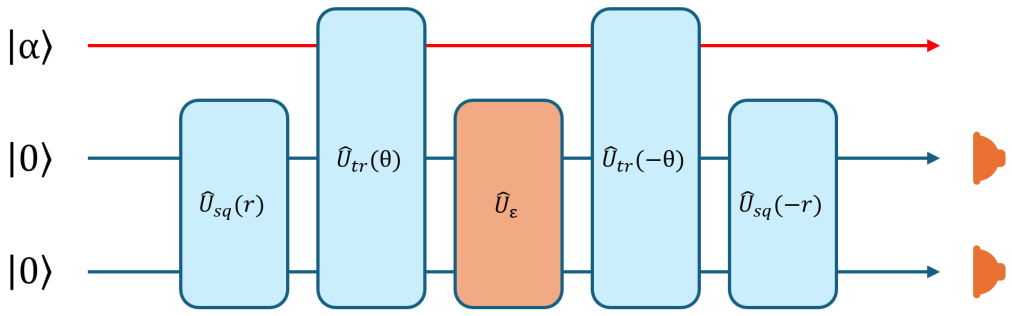

Figure 4.1: Circuit diagram representation of the quantum frequency interferometry scheme. The top red circuit represents the bulk of the BEC, initially in a coherent state, and the the other two circuits are the two side modes, initially in a vacuum state.

Chapter 5

BEC Gravimetry using the quantum frequency interferometre

We are now ready to discuss how the previous three chapters come together to form a novel method of BEC gravimetry, as proposed in the patent [1]. BEC gravimeters have been proposed before, see for example [66, 67], but their measurement scheme uses conventional interferometre techniques, contrary to our setup. Our aim is not necessarily just to enhance existing measurement precisions, but to include general relativistic effects in the quantum description of our quantum system. Our result will show how atoms at different points inside the condensate experience a different proper time, and how this affects the frequency spectrum of phonons once they are entangled. This is done by extending the work done on photonic systems in [3] to BEC systems. Therefore, this chapter will share similarities with that paper.

The work presented in this chapter expands on the contents of the patent. Here, we will consider a second BEC system as our reference to the phonon frequencies, unlike in the patent, in which an ideal point-like clock was used in the calculations. Furthermore, we will make use of the tritter operation in the scheme of a quantum frequency interferometre to improve the sensitivities. Although most of the work presented here is generally consistent with what is shown in the patent, several discrepancies were discovered. These will be pointed out and discussed as we progress through the calculations in this chapter.

We will start by describing the setup in detail and making some necessary

assumptions in 5.1. In sections 5.1.1 and 5.1.2, we then quantize the phonon fields inside the BEC in a curved background, finding an expression for their frequencies that includes general relativistic corrections. This will be followed by a detailed description of the metrology techniques utilised in 5.2. Finally, we evaluate the sensitivities obtainable for various measurement parameters, with a focus on measuring local gravitational acceleration.

5.1 Setup And Field Quantization

In our setup we consider a weakly-interacting atomic gas cooled below a critical temperature where the majority of the particles condense in their energetic ground state and form a BEC. We adopt the dynamics discussed in section 3.1. As such, we assume the Bose gas to be in the dilute regime, where we neglect any scattering processes other than pairwise interactions in the low-energy limit. The Bogoliubov approximation may be applied to our system implying that the macroscopically occupied ground state, the bulk of the Bose gas, may be treated classically, while the fluctuations about it behave quantum mechanically. These excitations are kept as quantum operators unlike the ground state which is described by a classical function. In the low energy limit the quasiparticles behave as phonons with frequency Ω.

To describe these phonons on a curved background we further impose the eikonal approximation, as described in section 3.2. The phonon fields obey the massless Klein-Gordon equation with the generalized d'Alembert operator

$$\Box \equiv \frac{1}{\sqrt{-G}}\partial_\mu(G^{\mu\nu}\sqrt{-G}\partial_\nu). \tag{5.1}$$

The corresponding metric $G_{\mu\nu}$ and its determinant $G = \det(G_{\mu\nu})$ is the acoustic metric, as in equation 3.46. We choose our reference frame, assuming isotropy, such that the spatial velocity flows vanish, i.e $u_\mu = u_\nu = (-1, 0, 0, 0)$. For the BECs that we are considering here, c_0^2/c^2 is of the order of 10^{-19}, therefore we can approximate $c_s \approx c_0$.

Taking the background metric to be the Schwarzschild metric describing spacetime curvature generated by the mass of Earth we get the effective

metric in isotropic Cartesian coordinates (ct, x, y, z)

$$G_{\mu\nu} = \rho \frac{c}{c_s} \left(1 + \frac{r_{\rm S}}{4\bar{r}}\right)^4 \text{diag}\left(-\frac{(1-\frac{\rm r_S}{4\bar{\rm r}})^2}{(1+\frac{\rm r_S}{4\bar{\rm r}})^6}\frac{\rm c_s^2}{\rm c^2}, 1, 1, 1\right). \tag{5.2}$$

In the above $r_{\rm S}$ is the Schwarzschild radius and $\bar{r} = (x^2 + y^2 + z^2)^{1/2}$. The spacetime curvature within the BEC is small when the distance from the BEC to the mass center is much larger than the Schwarzschild radius, i.e., $r_{\rm S}/\bar{r} \ll 1$. In this case we can expand the metric using a Taylor series around this parameter and neglect all contributions of higher than second order. We thus obtain the effective metric

$$G_{\mu\nu} = \rho \frac{c}{c_s} \left(\boldsymbol{\eta}_{bec} + \frac{r_{\rm S}}{\bar{r}}\,\mathbf{I}_{bec} + \frac{r_{\rm S}^2}{2\bar{r}^2}\text{diag}\left(-\rm c_s^2/c^2, \frac{3}{4}, \frac{3}{4}, \frac{3}{4}\right)\right), \tag{5.3}$$

where $\boldsymbol{\eta}_{bec} = \text{diag}(-\rm c_s^2/c^2, 1, 1, 1)$ and $\mathbf{I}_{bec} = \text{diag}\,(\rm c_s^2/c^2, 1, 1, 1)$. The phonon field can be written as a sum of the mode solutions ϕ_k of the massless Klein-Gordon equation

$$\psi = \sum_k \left[a_k\,\phi_k + a_k^*\,\phi_k^*\right]. \tag{5.4}$$

The mode numbers k are discrete because the solutions must vanish at the boundaries. The time-independent Fourier coefficients, a_k, are promoted to operators upon quantization [5].

We take the BEC to be in the uniform three-dimensional potential of an optical box trap. This has been shown to be experimentally achievable in [68], where they also cancelled the gravitational force on the atoms at a 10^{-4} level using a magnetic field. We take two such box cavities, one elongated along the x axis, perpendicular to the Earth's surface, and one along the z axis, parallel to the Earth's surface. We assume that their length in the elongated direction, L_x and L_z respectively, is sufficiently longer than the box's dimensions along the other two axes, so that in the ultracold limit for each BEC the momentum components of the phonons are only significant along the elongated axis and vanish in all other directions. This is because too much energy would be required to populate non-negligible excitations of those modes. We can then consider the BECs to be effectively $(1 + 1)$ dimensional.

The BECs are held at a constant radius from the centre of Earth. The vertical BEC, pointing along the x axis, experiences a proper acceleration

along its longitudinal axis, which is compensated for by the experimentalist. For the horizontal BEC, along the z axis, we can safely assume spacetime to be approximately flat along the cavity for the lengths considered here. This enables us to use the horizontal BEC as a reference in the laboratory frame. The vertical phonon frequencies will have additional terms compared to the horizontal case depending on their relative location and the local density perturbations due to an imperfect cancellation of the gravitational force.

The lengths of the BECs are determined by the distance between the sheet laser beams that form the end walls of the box trap. Assuming a Born rigid rod is holding the beams apart, the proper length of a BEC with ends at positions $x^\mu_{\rm P}$ and $x^\mu_{\rm Q}$ is given by

$$L = \int_{x^\mu_{\rm P}}^{x^\mu_{\rm Q}} d\sigma \sqrt{g_{\mu\nu} s^\mu(\sigma) s^\nu(\sigma)}\,, \tag{5.5}$$

where $s^\mu(\sigma)$ is the tangent vector to a space-like curve that connects the segments of the rod from the end at $x^\mu_{\rm P}$ to the end at $x^\mu_{\rm Q}$ chosen such that it lies inside the spatial slice defined by the rod's rest frame [31]. The proper lengths for horizontal and vertical cavities have been found for light clocks in the Schwarzschild metric in [3] and will have the same form in the BEC case.

Next, we will quantize the phonon fields in the two differently oriented BECs and show how their time evolutions differ.

5.1.1 The horizontal BEC

The BEC oriented along the z-direction is placed at $x = \bar{r}_0$ between points $z_{\rm l} = -l/2$ and $z_{\rm r} = l/2$, with coordinate length $l := z_{\rm r} - z_{\rm l} > 0$. We choose the coordinates (ct, z) in the effective $1+1$ dimensions and $\bar{r}(z) := (\bar{r}_0^2 + z^2)^{1/2}$. The effective metric components can be specified in equation 5.2, which after expanding up to second order in $z/\bar{r}_0$ and $r_{\rm S}/\bar{r}_0$ and to first order in their product yields

$$\boldsymbol{G}_{\rm h} \;=\; \rho \frac{c}{c_s} f_{\rm RS}(\bar{r}_0) {\rm diag}\left(-{\rm c}_{\rm s}^2/{\rm c}^2, \Sigma(\bar{\rm r}_0)\right)\,, \tag{5.6}$$

where

$$f_{\rm RS}(\bar{r}) := \left(1 - \frac{r_{\rm S}}{\bar{r}} + \frac{r_{\rm S}^2}{2\bar{r}^2}\right)\,,$$

is the redshift function and

$$\Sigma(\bar{r}) := \left(1 + \frac{2r_{\rm S}}{\bar{r}} + \frac{15r_{\rm S}^2}{8\bar{r}^2}\right),$$

is the spatial scale function. The proper length of the cavity oriented horizontally is $L_{\rm h} = f_{\rm RS}^{1/2}(\bar{r}_0)\Sigma^{1/2}(\bar{r}_0)l$. The end points in terms of the proper length are then

$$z_{\rm l} \approx -f_{\rm RS}^{-1/2}(\bar{r}_0)\Sigma^{-1/2}(\bar{r}_0)\frac{L_{\rm h}}{2}$$
$$z_{\rm r} \approx f_{\rm RS}^{-1/2}(\bar{r}_0)\Sigma^{-1/2}(\bar{r}_0)\frac{L_{\rm h}}{2}.$$

Before turning to the Klein-Gordon equation, we first make a simple conformal transformation to coordinates $(\tilde{x}^0, \tilde{z})$, where $\tilde{x}^0 := c_s t$ and $\tilde{z} := \Sigma^{1/2}(\bar{r}_0)z$. This can be done since the solutions to the Klein-Gordon equation are conformally-invariant in 1+1 dimensions. In these conformal coordinates, the effective metric now takes the diagonal form

$$\tilde{\boldsymbol{G}}_{\rm h} \;=\; \rho\frac{c}{c_s}f_{\rm RS}(\bar{r}_0)\mathrm{diag}\,(-1,1)\,. \tag{5.7}$$

We are now able to easily solve the Klein-Gordon equation with Dirichlet boundary conditions requiring that the solutions vanish at the ends of the cavities $\psi_{\rm h}(\tilde{x}^0, \tilde{z}_{\rm l}) = \psi_{\rm h}(\tilde{x}^0, \tilde{z}_{\rm r}) = 0$. The mode solutions, $\phi_{{\rm h},k}$, normalized with respect to the Klein-Gordon inner product are

$$\phi_{{\rm h},k}(\tilde{x}^0, \tilde{z}) := \frac{1}{\sqrt{\pi k}}e^{-i\Omega_{{\rm h},k}t}\sin\left(\frac{\Omega_{{\rm h},k}}{c_s}(\tilde{z} - \tilde{z}_{\rm l})\right), \tag{5.8}$$

where k is a positive integer. The horizontal phonon frequencies $\Omega_{{\rm h},k}$ are given by

$$\Omega_{{\rm h},k} = \frac{c_s\pi k}{\tilde{z}_{\rm r} - \tilde{z}_{\rm l}} = \frac{c_s\pi k}{L_{\rm h}}f_{\rm RS}^{1/2}(\bar{r}_0). \tag{5.9}$$

The field $\psi_{\rm h}$ is quantized in the $\phi_{{\rm h},k}$ basis by associating annihilation and creation operators $\hat{a}_{{\rm h},k}$ and $\hat{a}^\dagger_{{\rm h},k}$ to the positive and negative solutions, $\phi_{{\rm h},k}$ and $\phi^*_{{\rm h},k}$ respectively. The quantized phonon field in the horizontally oriented BEC is then

$$\hat{\psi}_{\rm h}(\tilde{x}^0, \tilde{z}) = \sum_k \left\{\hat{a}_{{\rm h},k}\,\phi_{{\rm h},k}(\tilde{x}^0, \tilde{z}) + \hat{a}^\dagger_{{\rm h},k}\,\phi^*_{{\rm h},k}(\tilde{x}^0, \tilde{z})\right\}. \tag{5.10}$$

The creation and annihilation operators satisfy the canonical commutation relations $[\hat{a}_{{\rm h},k}, \hat{a}^\dagger_{h,k'}] = \delta_{k,k'}$, while all other commutators vanish.

5.1.2 The vertical BEC

The second, vertical BEC is placed along the x axis, perpendicular to the first one. It is convenient to choose the origin for the coordinates to be the point where the horizontal BEC intersects the vertical one at $x = \bar{r}_0$. In these effectively 1+1 dimensional coordinates (ct, x'), we have defined $x' = x - \bar{r}_0$, and assume that the ends of the BEC are located at $x'_b = -l(1+\chi)/2$ and $x'_t = l(1-\chi)/2$. In this we introduced χ, which specifies the theoretical point of intersection of the two BEC cavities with $-1 \leq \chi \leq 1$. When the intersection is at the middle of the vertical cavity $\chi = 0$, while $\chi = -1$ and $\chi = 1$ correspond to the intersection being at the bottom and top points respectively. This is a useful reference in the laboratory frame to define the frequencies measured. Note that in the patent only the special case of $\chi = -1$ is considered.

As reported in [68, 69], we account for the external potential applied to compensate for the gravitational force on the atoms. The experimenters tuned the magnetic field gradient, B', so it cancelled the gravitational force as $\mu_B B' = mg$ to 10^{-4} level, where μ_B is the Bohr magneton. The applied potential energy can then be effectively expressed as the Newtonian gravitational potential energy

$$V_B = mgx' = -m\frac{GM}{\bar{r}_b^2}x' = -\frac{mc^2}{2}\frac{r_{\mathrm{S}}x'}{\bar{r}_b^2}, \tag{5.11}$$

where $r_{\mathrm{S}} = 2GM/c^2$ was used. This is in conflict with the patent, where the same potential is quoted in statement 0166 to be

$$V_B^p = -\frac{m^2}{\hbar^2}\frac{r_{\mathrm{S}}x'}{\bar{r}_b^2}u_0^2 \approx \frac{m^2c^2}{\hbar^2}\frac{r_{\mathrm{S}}x'}{\bar{r}_b^2}. \tag{5.12}$$

It is unclear how this was derived, but a dimensional analysis reveals that this quantity has dimensions of 1 over length squared:

$$\mathrm{dimV_B^p} = \frac{\mathrm{M^2L^2T^{-2}}}{\mathrm{M^2L^4T^{-2}}}\frac{\mathrm{L*L}}{\mathrm{L^2}} = \mathrm{L^{-2}}. \tag{5.13}$$

As the expected dimension is that of energy, which it is for V_B, this could be due to a typo. Nonetheless, using the form obtained for V_B here, the same expression for the density perturbation as in the patent may be derived, which will be shown next.

The Earth's gravitational potential at $\bar{r}_0$ would be recovered if $\bar{r}_0 = \bar{r}_b$ was matched perfectly. However, we are interested in the case when the cancellation is not perfect, and the applied potential is tuned away slightly from $r_S/\bar{r}_0^2$ to $r_S/\bar{r}_b^2$, resulting in a new effective potential, ΔV. We write the shift in the BEC density as $\rho' = \rho_0(1 + \delta_\rho)$. Using the Thomas-Fermi result from section 3.1.3, the ground state density of the condensate in a uniform potential is given by

$$\rho_0 = \frac{\mu}{\lambda}. \tag{5.14}$$

Here, we introduced the chemical potential of the bulk, $\mu = mc_s^2$, making use of the approximation $c_0 \approx c_s$. The new density is then written as

$$\rho' = \frac{1}{\lambda}(\mu - \Delta V) = \frac{\mu}{\lambda}(1 + \delta_\rho). \tag{5.15}$$

Rearranging for the density perturbation gives

$$\delta_\rho = -\frac{\Delta V}{\mu} = \frac{r_S c^2}{2c_s^2}|D_v|x, \tag{5.16}$$

where $D_v := 1/\bar{r}_0^2 - 1/\bar{r}_b^2$ is what we will call the tuning parameter. Since particle number is assumed to be conserved, $\int_{x'_b}^{x'_t} dx' \delta_\rho = 0$ must hold. Applying these boundary conditions on the density perturbation we get

$$\delta_\rho = \frac{r_S c^2}{2c_s^2}|D_v|(x' + \frac{l\chi}{2}). \tag{5.17}$$

This is consistent with the expression for the same quantity of the patent in statement 0167.

The effective metric with the perturbed density now takes the form

$$G_{\mu\nu} = \rho_0 \frac{c}{c_s}(1 + \delta_\rho)^{\frac{1}{2}} \left(1 + \frac{r_S}{4\bar{r}}\right)^4 \\ \text{diag}\left(-\frac{(1 - \frac{r_S}{4\bar{r}})^2}{(1 + \frac{r_S}{4\bar{r}})^6}\frac{c_s^2}{c^2}(1 + \delta_\rho), 1\right), \tag{5.18}$$

with $\bar{r}(x') := \bar{r}_0 + x'$. This time, the effective $1+1$ dimensional metric inside the vertical BEC is expanded up to fourth order in $r_S/\bar{r}_0$ and $x'/\bar{r}_0$ and to second order in their product. However, in the obtained expression we neglect all terms that are lower in order of magnitude than $r_S x'/\bar{r}_0^2 \sim 10^{-19}$.

Note that the same procedure could be done for the horizontal metric and it would not change the results in that section, as the second order expansion would be recovered exactly. In the vertical case on the other hand, we retain terms proportional to δ_ρ^2 this way, which greatly enhances the precision of the approximation. The resulting metric has the non-zero components

$$\boldsymbol{G}_{\mathrm{v},00} = -\rho_0 \frac{c_s}{c} f_{\mathrm{RS}}(\bar{r}_0) \left(1 + \frac{r_{\mathrm{S}} x'}{\bar{r}_0^2} + \frac{3\delta_\rho}{2} + \frac{3\delta_\rho^2}{8}\right), \tag{5.19}$$

$$\boldsymbol{G}_{\mathrm{v},11} = \rho_0 \frac{c}{c_s} f_{\mathrm{RS}}(\bar{r}_0) \Sigma(\bar{r}_0) \left(1 - \frac{r_{\mathrm{S}} x'}{\bar{r}_0^2} + \frac{\delta_\rho}{2} - \frac{\delta_\rho^2}{8}\right). \tag{5.20}$$

Next, similar to the horizontal case, a conformal transformation to coordinates $(\tilde{x}^0, \tilde{x})$ is made in order to solve the Klein-Gordon equation. The space-like coordinate is calculated as

$$\begin{aligned} \tilde{x} &= \int_0^{x'} dx'' \sqrt{\frac{\boldsymbol{G}_{\mathrm{v},11}(x'')}{|\boldsymbol{G}_{\mathrm{v},00}(x'')|}} \\ &\approx \Sigma^{1/2}(\bar{r}_0) x' \left(1 - \frac{r_{\mathrm{S}} x'}{2\bar{r}_0^2} - \frac{\delta'_\rho}{4}(x' + l\chi) \right. \\ &\qquad \left. + \frac{\delta_\rho'^2}{8}\left(x'^2 + \frac{3l}{2}\chi(x' + \frac{l}{2}\chi)\right)\right). \end{aligned} \tag{5.21}$$

In the above, we labeled the first derivative of the density perturbation as $\delta'_\rho := \frac{r_{\mathrm{S}} c^2}{2c_s^2}|D_v|$. In the new conformal coordinates, the metric is

$$\tilde{\boldsymbol{G}}_{\mathrm{v}} = \rho_0 \frac{c}{c_s} f_{\mathrm{RS}}(\bar{r}_0) \left(1 + \frac{r_{\mathrm{S}} x'}{\bar{r}_0^2} + \frac{3\delta_\rho}{2} + \frac{3\delta_\rho^2}{8}\right) \mathrm{diag}\,(-1, 1). \tag{5.22}$$

The Klein-Gordon equation is now easily solved with the Dirichlet boundary conditions, which are $\psi_{\mathrm{v}}(\tilde{x}^0, \tilde{x}_b) = \psi_{\mathrm{v}}(\tilde{x}^0, \tilde{x}_{\mathrm{t}}) = 0$, and the mode solutions yield

$$\phi_{\mathrm{v},k}(\tilde{x}^0, \tilde{x}) := \frac{e^{-i\Omega_{\mathrm{v},k} t}}{\sqrt{\pi k}} \sin\left(\frac{\Omega_{\mathrm{v},k}}{c_s}(\tilde{x} - \tilde{x_{\mathrm{b}}})\right), \tag{5.23}$$

where the vertical phonon frequencies are $\Omega_{\mathrm{v},k} := \frac{c_s \pi k}{\tilde{x}_{\mathrm{t}} - \tilde{x}_{\mathrm{b}}}$. These can be expressed in terms of the proper length using the result

$$l = f_{\mathrm{RS}}^{-1/2}(\bar{r}_0) \Sigma^{-1/2}(\bar{r}_0)\, L_{\mathrm{v}} \left(1 - \frac{r_{\mathrm{S}}\, L_{\mathrm{v}}}{4\bar{r}_0^2}\chi\right), \tag{5.24}$$

from [3], which yields

$$\Omega_{\mathrm{v},k} \approx \frac{c_s \pi k}{L_\mathrm{v}} f_{\mathrm{RS}}^{1/2}(\bar{r}_0) \left(1 - \frac{\delta_\rho'^2 L_\mathrm{v}^2}{32} - \frac{r_\mathrm{S} L_\mathrm{v}}{4\bar{r}_0^2}\chi\right). \tag{5.25}$$

The linear density perturbation terms vanish to the relevant order due to their boundary conditions. To quantize the field, we introduce creation and annihilation operators $\hat{a}_{\mathrm{v},k}^\dagger, \hat{a}_{\mathrm{v},k}$ that satisfy the canonical commutation relations $[\hat{a}_{\mathrm{v},k}, \hat{a}_{\mathrm{v},k'}^\dagger] = \delta_{k,k'}$, while all other commutators vanish. The quantized phonon field $\hat{\psi}_\mathrm{v}$ in the vertical BEC is given by

$$\hat{\psi}_\mathrm{v}(\tilde{x}^0, \tilde{x}) = \sum_k \left\{\hat{a}_{\mathrm{v},k}\, \phi_{\mathrm{v},k}(\tilde{x}^0, \tilde{x}) + \hat{a}_{\mathrm{v},k}^\dagger\, \phi_{\mathrm{v},k}^*(\tilde{x}^0, \tilde{x})\right\}. \tag{5.26}$$

Comparing these results to the ones in the patent, equation 5.21 is in disagreement with equation 40 in statement 0174, where it seems likely that components $\boldsymbol{G}_{\mathrm{v},00}$ are used instead of $\boldsymbol{G}_{\mathrm{v},11}/\boldsymbol{G}_{\mathrm{v},00}$ in the calculation. Despite that, the result in equation 46 of statement 0176 is almost entirely consistent with the one obtained here in equation 5.25, with the only difference being a factor of $1/2$ in the term proportional to $\delta_\rho'^2$.

5.2 Quantum Metrology

We now discuss how one might use the vertically placed system to measure certain parameters of interest. For our setup we consider the quantum frequency interferometry scheme outlined in 4.3. In this type of interferometry, unlike in conventional spatial interferometers, the frequency modes of interest remain in physical contact with each other. This allows us to act on our system with global unitary channels, which imprint the parameters to be estimated and improve sensitivites by preparing entangled states. Below, we show an implementation of this scheme on our BEC setup and calculate bounds on the estimation precisions of proper time, gravity, and also the dynamical Casimir effect. We will consider Gaussian operations and input states only and make use of the covariance matrix formalism.

Our frequency interferometry scheme consists of three modes. The first mode we take to be the bulk of the BEC (the phononic ground state). We assume that this mode is initially in a coherent state and call it the

pump mode. The other two modes are the phononic side modes representing collective excitations in the BEC. The side modes are assumed to be initially unpopulated so they are both described by the vacuum state. To populate them, we act on the state with a two-mode squeezing operation $\hat{U}_{sq}(r) = \exp\{re^{i\vartheta_{sq}}(\hat{a}_n^\dagger \hat{a}_m^\dagger - \hat{a}_n \hat{a}_m)\}$. In the covariance matrix formalism, the state of the full system is then given by $\mathbf{S}_s\mathbf{d}_0$ and $\mathbf{S}_s\boldsymbol{\sigma}_0\mathbf{S}_s^T$ where $\mathbf{S}_s$ is the symplectic matrix of this squeezing unitary and $\mathbf{d}_0$ and $\boldsymbol{\sigma}_0$ are the displacement and covariance matrices of the initial coherent state respectively. This is followed by a tritter operation with symplectic matrix $\mathbf{S}_{tr}$, generated by the Hamiltonian

$$\hat{H}_{tr} = \frac{\hbar\theta}{\sqrt{2}}\Big[e^{i\vartheta}\hat{a}_0^\dagger(\hat{a}_n + \hat{a}_m) + e^{-i\vartheta}\hat{a}_0(\hat{a}_n^\dagger + \hat{a}_m^\dagger)\Big]. \tag{5.27}$$

This is a three-mode mixing channel that mixes the side modes with the pump mode, further improving sensitivities.

The two operations discussed so far are brought about using suitable external potential fields. These are then turned off and the BEC is allowed to evolve freely in the box potential under the effect of gravity and the gravity compensating potential. This is represented by a two-mode phase-shift channel acting on the side modes

$$\hat{U}_\epsilon = e^{-\frac{i}{2}(\omega_n+\omega_m)\tau_0(\hat{a}_n^\dagger\hat{a}_n + \hat{a}_m^\dagger\hat{a}_m)}. \tag{5.28}$$

This has the effect of imprinting a parameter, ϵ, that is to be estimated with the phases ω_n and ω_m of the respective states. This is different from a spatial interferometer where the modes follow different trajectories and they each pick up a phase resulting in sensitivity to the relative phase $\omega_n - \omega_m$. Instead, this setup is sensitive to the total unitary transformation and therefore to $\omega_n + \omega_m$. The corresponding symplectic matrix is

$$\mathbf{S}_\epsilon = \begin{pmatrix} 1 & 0 & 0 & 0 & 0 & 0 \\ 0 & e^{-\frac{i}{2}(\omega_n+\omega_m)\tau_0} & 0 & 0 & 0 & 0 \\ 0 & 0 & e^{-\frac{i}{2}(\omega_n+\omega_m)\tau_0} & 0 & 0 & 0 \\ 0 & 0 & 0 & 1 & 0 & 0 \\ 0 & 0 & 0 & 0 & e^{\frac{i}{2}(\omega_n+\omega_m)\tau_0} & 0 \\ 0 & 0 & 0 & 0 & 0 & e^{\frac{i}{2}(\omega_n+\omega_m)\tau_0} \end{pmatrix}. \tag{5.29}$$

Finally, to recombine the three modes and create interference, the inverse of the tritter and squeezing channels are applied, after which a number-sum measurement is performed on the side modes. The state of the full interferometer is then defined by $\mathbf{d} = \mathbf{S}\mathbf{d}_0$ and $\boldsymbol{\sigma} = \mathbf{S}\boldsymbol{\sigma}_0\mathbf{S}^T$, where $\mathbf{S} := \mathbf{S}_-\mathbf{S}_\epsilon\mathbf{S}_+$ with $\mathbf{S}_- := \mathbf{S}_s(-r)\mathbf{S}_{tr}(-\theta)$, $\mathbf{S}_+ := \mathbf{S}_{tr}(\theta)\mathbf{S}_s(r)$ and $\mathbf{S}_\epsilon$ being the state evolution under gravity.

In measuring ϵ the precision is bounded by the quantum Cramér-Rao bound [70]

$$\Delta\epsilon \geq \frac{1}{\sqrt{\mathcal{M}\, H(\epsilon)}} \tag{5.30}$$

where $\mathcal{M}$ is the number of measurements and $H(\epsilon)$ the quantum Fisher information. It was shown in [71] that for the scheme we are considering here, the impurities of the Gaussian state can be safely neglected, thus the quantum Fisher information is written as in equation 4.19

$$H(\epsilon) = \frac{1}{4}\mathrm{Tr}\left[\left(\boldsymbol{\sigma}(\epsilon)^{-1}\partial_\epsilon\boldsymbol{\sigma}(\epsilon)\right)^2\right] + 2\partial_\epsilon\boldsymbol{d}^\dagger(\epsilon)\boldsymbol{\sigma}^{-1}(\epsilon)\partial_\epsilon\boldsymbol{d}(\epsilon). \tag{5.31}$$

Performing this calculation yields

$$\begin{aligned} H(\epsilon) =& \frac{1}{4}\left(\partial_\epsilon((\omega_n+\omega_m)\tau_0)\right)^2 \Bigg[\sin^2(2\theta)\sinh^2 r \\ &+ 2(1+\cos^4\theta)\sinh^2(2r) + |\alpha_0|^2\Bigg(4\sin^4\theta \\ &+ \cosh(2r)\sin^2(2\theta) - \sinh(2r)\cos\nu_P\sin^2(2\theta)\Bigg)\Bigg], \end{aligned} \tag{5.32}$$

where:

$$\nu_P := 2(\vartheta - \vartheta_P) + \vartheta_{sq}. \tag{5.33}$$

In the above $|\alpha_0|^2 = N_0$ is the number of particles in the pump beam after the squeezing and ϑ_P is the phase of the pump.

We set our experimental parameters based on a ^{87}Rb BEC trapped in a uniform potential, as it was demonstrated in [68, 69]. In his PhD thesis, Paul Juschitz discusses the different experimental approaches for creating the optimal BEC for gravitational experiments and analyses the parameters [72].

Parameter	Symbol	Value
Length of BEC	L	$70\,\mu$m
Speed of sound in BEC	c_s	$0.002\,$m/s
Distance from centre of Earth	$\bar{r}_0$	$6.37 \times 10^6\,$m
Mode numbers	n, m	$2, 3$
Number of particles in BEC	N_0	6×10^5
Squeezing parameter	r	1.9
Tritter angle	θ	$0.81\,$rad
Interaction time	τ_{int}	$0.2\,$s

Table 5.1: Experimental parameters considered for a ^{87}Rb BEC trapped in a box potential, used in calculating the sensitivities.

He concludes for the setup we are considering here that the optimal mode numbers are those no greater than 3. Furthermore, he sets a theoretical upper bound on the squeezing parameter, which is $r = 1.9$. Above this value the number of phonons created start to get too large, effectively destroying the BEC. This corresponds to a squeezing factor of -13.3 Db[1]. While squeezing has not yet been realised for a BEC in the box trap, various other methods demonstrated squeezing up to about -8 Db [74, 75, 76, 77], not too far from our theoretical limit. While its implementation remains an experimental challenge, we base our calculations on the optimistic value of $r = 1.9$. Setting the phases to be most optimal, $\nu_P = \pi/2$, we find the optimal tritter angle to be $\theta = 0.81$ radians. We also set the point of intersection to be most optimal, i.e. $\chi = 1$. The parameters are summarised in table 5.1, assuming a setup in which $L_{\text{h}} = L_{\text{v}} := L$. We take the interaction time with the parameter encoding channel $\hat{U}_\epsilon$ to be 0.2 seconds, safely below the lifetime of the phonons reported for this BEC, which was 0.3 seconds [68, 69].

For the eikonal approximation to be valid, we require that the gradient of the BEC density perturbation remains small compared to the wavelength of the phonons

$$\left|\frac{\partial_{x'}\rho'}{\rho'}\right| \approx \left|\delta'_\rho\right| \ll \frac{2\pi c_s}{\Omega_k} \approx \frac{2L}{k} \sim 10^{-5}\text{m}. \tag{5.34}$$

[1]Calculated as $10\log_{10}(2\sinh^2 r)$ [73, 72]

This in turn restricts D_v as

$$|D_v| \ll \left(\frac{r_{\mathrm{S}}c^2}{2c_s^2}\right)^{-1} \frac{2L}{k} \sim 10^{-25}\,\mathrm{m}^{-2}, \tag{5.35}$$

or equivalently

$$\frac{\bar{r}_0}{\bar{r}_b} \ll 1 \pm 10^{-11}. \tag{5.36}$$

This means that the experimenter must tune the gravity compensating potential so as to match the local gravitation to within picometre precision, otherwise the density variations in space are too large on the scales of the phonon wavelength, rendering the effective metric invalid. This severe limitation doesn't only pose a feasibility problem to the experimenter, but it also significantly raises the relative error. Therefore there is a balance to be struck here; cancelling gravity enough for the model to remain valid, but not too much so that gravity leaves an effect that is measurable.

5.2.1 Estimating Proper Time

One could consider proper time as the encoded parameter, turning the setup into a BEC clock. We found that the frequencies for the horizontal and vertical BECs respectively for mode number k are given by

$$\Omega_{\mathrm{h},k} = \frac{c_s \pi k}{L_h} f_{\mathrm{RS}}^{1/2}(\bar{r}_0), \tag{5.37}$$

$$\Omega_{\mathrm{v},k} = \frac{c_s \pi k}{L_{\mathrm{v}}} f_{\mathrm{RS}}^{1/2}(\bar{r}_0) \left(1 - \frac{\delta_\rho'^2 L_{\mathrm{v}}^2}{32} - \frac{r_{\mathrm{S}} L_{\mathrm{v}}}{4\bar{r}_0^2}\chi\right). \tag{5.38}$$

The proper time of an observer static at a fixed radial position r in Schwarzschild spacetime is given by $\tau(r) = f(r)^{1/2} t$ with respect to the coordinate time t. We also define the proper time $\tau_0 := f_{\mathrm{RS}}^{1/2}(\bar{r}_0)\, t$, measured by an ideal point-like clock at $\bar{r}_0$. With respect to the point $\bar{r}_0$, the frequencies measured in the laboratory reference frame are given by $\omega_{\mathrm{h}} \tau_0 = \Omega_{\mathrm{h}}\, t$ and $\omega_{\mathrm{v}}\, \tau_0 = \Omega_{\mathrm{v}}\, t$. This yields

$$\omega_{\mathrm{h},k}(\bar{r}_0) = \frac{c_s \pi k}{L} \tag{5.39}$$

$$\omega_{\mathrm{v},k}(\bar{r}_0) = \omega_{\mathrm{h},k}(\bar{r}_0) \left(1 - \frac{\delta_\rho'^2 L^2}{32} - \frac{r_{\mathrm{S}} L}{4\bar{r}_0^2}\chi\right). \tag{5.40}$$

The bounds on the error in estimating the proper time in the horizontal and vertical BECs are related as

$$\Delta_{\mathrm{v}}\tau_0 = \Delta_{\mathrm{h}}\tau_0 \left(1 + \frac{r_{\mathrm{S}}L}{4\bar{r}_0^2}\chi + \frac{\delta_\rho'^2 L^2}{32}\right), \tag{5.41}$$

expanded to the relevant order. Thus, we can see how the proper time changes inside the vertical BEC clock compared to the horizontal reference BEC clock depending on their relative position, χ. This shows how the atoms inside the BEC experience different proper times depending on their height.

The optimal bound to the relative error $\delta(\tau_0) := |\Delta\tau_0|/|\tau_0|$ for the vertically placed BEC is found to be

$$\delta_{\mathrm{v}}(\tau_0) = \frac{2}{(\omega_{\mathrm{v},n} + \omega_{\mathrm{v},m})\tau_0\sqrt{\mathcal{M}\,H'(r,\theta)}}, \tag{5.42}$$

where

$$\begin{aligned} H'(r,\theta) = \sin^2(2\theta)\sinh^2 r + 2(1+\cos^4\theta)\sinh^2(2r) \\ + |\alpha_0|^2\left(4\sin^4\theta + \cosh(2r)\sin^2(2\theta)\right). \end{aligned} \tag{5.43}$$

For a single measurement we get $\delta(\tau_0) = 5.9 \times 10^{-7}$. This can be improved by a factor of 10 for every factor of 100 times the measurement is carried out. The light clock discussed in [3] significantly outperforms the BEC clock presented here. This is expected due to the comparatively slow speed of sound in the BEC relative to the speed of light.

5.2.2 Estimating Local Gravitation

There are at least two ways how one might treat local gravity as the encoded parameter. One could estimate it directly, considering $\epsilon = g := GM/\bar{r}_0^2$, or indirectly through estimating the Scwarzschild radius, $\epsilon = r_{\mathrm{S}} := 2GM/c^2$, as done in the paper for the light clock case [3] and in the patent. The two quantities relate to each other as $r_{\mathrm{S}} = 2\bar{r}_0^2 g/c^2$. The vertical frequency can be expressed in terms of the local accelerations due to gravity and the gravity compensating potential, g and a respectively, as

$$\omega_v(\bar{r}_0) = \omega_{\mathrm{h}}(\bar{r}_0)\left(1 - \frac{L^2}{32c_s^4}(g-a)^2 - \frac{Lg}{2c^2}\chi\right). \tag{5.44}$$

Therefore, the error bound in estimating local gravitation in the vertical BEC can be expressed as

$$\begin{aligned}\delta_{\mathrm{v}}(g) &= \frac{2}{g\tau_0 \frac{\mathrm{d}}{\mathrm{d}g}(\omega_{\mathrm{v},n} + \omega_{\mathrm{v},m})\sqrt{\mathcal{M}\, H'(r,\theta)}} \\ &= \frac{32 c_s^3 c^2}{(n+m)\pi\tau_0 g\left(Lc^2 GM|D_v| + 8c_s^4\chi\right)\sqrt{\mathcal{M}H'(r,\theta)}},\end{aligned} \tag{5.45}$$

where we used $|g - a| = GM|D_v|$. Note that we dropped the negative signs from the frequency 5.44, as the expression has been squared and square rooted.

To make an exact comparison with the patent, we can recast the above in terms of r_{S} in a form consistent with the one used in the patent. Firstly, note that in calculating these sensitivities the patent considers an ideal point-like clock at infinity as the reference, therefore we set $\chi = 0$. Second, the estimating channel comprises simply of a single-mode squeezed state without the tritter, which leads to a slightly different quantum Fisher information $H'(r)$. Nonetheless, taking these changes into account we find that our expression for the relative error bound on the proper time, $\delta(\tau_0)$ 5.42, is consistent with the equivalent expression of the patent presented in equation 65 of statement 0187. Following the methods of the patent, we now express the relative error bound for r_{S} in the vertical BEC in terms of the relative error bound for τ_0 in the horizontal BEC as

$$\begin{aligned}\delta_{\mathrm{v}}(r_{\mathrm{S}}) &= \delta_{\mathrm{h}}(\tau_0)\frac{\tau_0}{r_{\mathrm{S}}}\frac{\omega_{\mathrm{h},n+m}}{\left|\frac{\mathrm{d}}{\mathrm{d}r_{\mathrm{S}}}(\omega_{v,n+m}\,\tau_0)\right|} \\ &= \frac{4}{r_{\mathrm{S}}L}\frac{c_s^2}{c^2}\frac{8}{\delta'_\rho L}\delta_{\mathrm{h}}(\tau_0)\frac{1}{|D_v|}.\end{aligned} \tag{5.46}$$

This is similar but not the same as the equivalent expression in equation 78 of statement 0200 of the patent, with two discrepancies. The first is that the expression derived above is missing a factor of $\sqrt{2}$ compared to the patent's result. This is simply due to the patent considering an ideal point-like clock as the reference, affecting how the sensitivities combine, as discussed in statement 0192. However, the second discrepancy is significant and severe. Specifically, the factor $1/|D_v|$ is obtained instead of $\bar{r}_0^2 V_B^p$. Performing a dimensional analysis one finds the expression for $\delta_{\mathrm{v}}(r_{\mathrm{S}})$ derived here to be dimensionless, as would be expected for the relative error. However, the expression in the patent is only dimensionless if V_B^p is dimensionless

(as all other components combined are dimensionless). But previously, in equation 5.13, it was found that V_B^p has dimensions of 1 over length squared. It is possible that the form of V_B^p is wrong in the patent and it is actually dimensionless, or that $\bar{r}_0^2$ is included by mistake and V_B^p has a similar (or potentially the same) role as what is denoted by D_v here.

The patent reports a value of 10^{-16} for the relative error bound in statement 0211. According to the above expression 5.46, and the parameters defined in the patent in statement 0195 and 0222, this corresponds to $|D_v| \sim 10^{-13}$, which violates the eikonal approximation conditions established in equation 5.35. The patent makes no mention of this approximation or why it is ignored. In fact, this could be viewed as the greatest discrepancy between the work in the patent and the work presented here. With only the typo corrections and small adjustments discussed, a similar result for the relative error bound obtained in the patent could be justified here. However, imposing the necessary assumption first mentioned in 3.40, then spelled out in the relevant format in 5.34, suggests that these results lie outside the regime where the model used can be considered valid.

Calculating the relative error bound in a single measurement of r_{S} for the light clock presented in [3] with the parameters used there, we obtain $\delta_{\mathrm{light}}(r_{\mathrm{S}}) = 9.7 \times 10^6$. The BEC setup outlined in this thesis would outperform this as long as $|D_v| > 10^{-21}$. This, however, still lies outside of the permitted bound according to the condition 5.35.

To compare the performance of our BEC gravimetre to commercial competitors, we calculate the sensitivities as $\Delta_{\mathrm{v}} g / \sqrt{\mathcal{M}/\mathrm{sec}}$ and use the conventional units of $\mathrm{Gal}/\sqrt{\mathrm{Hz}}$. We are assuming a sampling rate of 2Hz, meaning two measurements taken every second. The exact value depends on how fast the experiment can be set up after each measurement. Figure 5.1 shows these sensitivities for different values of $|D_v|$ for two different tritter angles. When the tritter is tuned to the optimal angle, an improvement of 2 orders of magnitude is observed compared to when the tritter is turned off. The vertical red line represents the upper limit on the tuning parameter. According to the condition 5.35, all sensitivities right of the red line are prohibited if the eikonal approximation were to remain valid. This condition heavily limits the sensitivities achievable.

In comparison, the state of the art commercial quantum gravimetre, μQuans, reports a sensitivity of 5×10^{-5} $\mathrm{Gal}/\sqrt{\mathrm{Hz}}$ [78]. It is an atom interferometre using laser cooled atoms, with both the control unit and sensor

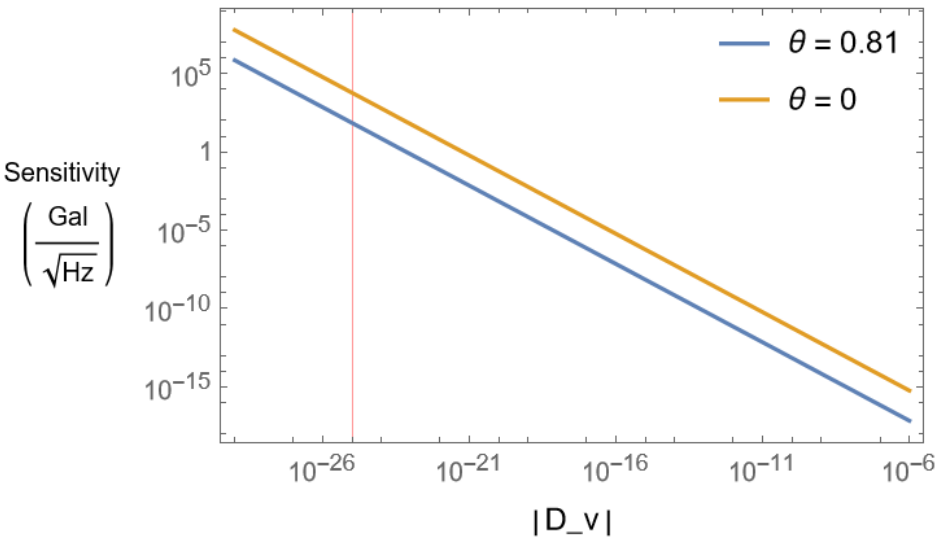

Figure 5.1: Sensitivities on a single measurement of g for different values of the tuning parameter. The yellow line corresponds to the measurement scheme without the tritter, and the blue line to when the tritter angle is most optimal. The vertical red line indicates the restricting threshold on the tuning parameter due to the eikonal approximation.

less than a metre tall. Its level of performance in terms of sensitivity corresponds to $|D_v| \sim 10^{-18}$ in our BEC setup. This means that the sensitivity of our BEC gravimetre scheme with the parameters defined here falls short by about 8 orders of magnitude from the current leading commercial quantum technology.

5.2.3 Estimating The Dynamical Casimir Effect

Our setup may also be used to measure the dynamical Casimir effect, induced by the relativistic motion of the end walls of the box potential confining the BEC. The transformation of quantum field states under this effect in curved spacetime was discussed in a paper by Maximilian Lock and Ivette Fuentes [4], where they also proposed that their predictions could be tested with a vertically oriented BEC. Here we quantify the sensitivities achievable with such a setup, but to keep things simple, we consider just a single phonon mode. Then, we discuss how one might apply the quantum frequency inter-

ferometry scheme to improve the sensitivities.

Suppose the experimenter moves the top end of the vertical BEC in an oscillatory way, so that its coordinate position is

$$x_t = x_{t,0} + A\sin(\nu t). \tag{5.47}$$

During this motion, the proper length of the BEC oscillates as

$$L(t) = L_0 + \tilde{A}\sin(\nu t). \tag{5.48}$$

We assume that the amplitude of the oscillation is small compared to the length of the BEC. The two amplitudes are then related as

$$A = \frac{\sqrt{f_{\mathrm{RS}}(x_{t,0})}}{\sqrt{f_{\mathrm{RS}}(x_{t,0})} + \frac{r_{\mathrm{S}}}{2x_{t,0}}}\tilde{A}. \tag{5.49}$$

Furthermore, we must also assume that the speed of oscillations is much slower than the speed of sound in the BEC. This, in turn, sets an upper limit on the amplitude of the oscillation.

As a result of this boundary motion, the phonon mode transforms under the combination of a phase shift and a single mode squeezing channel, as described in [4]. This implies the creation of phonons due to the relativistic motion of the boundaries, which in principle can be measured with this setup.

The state of the full scheme is then $\mathbf{d} = \mathbf{S}_\epsilon \mathbf{d}_0$ and $\boldsymbol{\sigma} = \mathbf{S}_\epsilon \boldsymbol{\sigma}_0 \mathbf{S}_\epsilon^T$, where $\mathbf{S}_\epsilon = \mathbf{R}(\omega_k t)\mathbf{S}_{ss}(r_{dc})$. The single mode phase shift and squeezing symplectic matrices, $\mathbf{R}$ and $\mathbf{S}_{ss}$ are defined in equations 4.27 and 4.28 respectively. The matrix elements of $\mathbf{S}_\epsilon$ are the Bogoliubov coefficients

$$\mathbf{S}_\epsilon = \begin{bmatrix} \alpha & \beta \\ \beta^* & \alpha^* \end{bmatrix}, \tag{5.50}$$

defined by the inner products

$$\begin{aligned} \alpha &= \Big(\phi_{\mathrm{v},k}(x^0, x; t_0 + \delta t, x_{t,0} + \delta x), \phi_{\mathrm{v},k}(x^0, x; t_0, x_0)\Big) \\ \beta &= -\Big(\phi_{\mathrm{v},k}(x^0, x; t_0 + \delta t, x_{t,0} + \delta x), \phi^*_{\mathrm{v},k}(x^0, x; t_0, x_0)\Big). \end{aligned} \tag{5.51}$$

These inner products are evaluated in [4] and the results can be related to r_{dc}. Specifically, in the case when the experimenter drives the boundary at

the resonance $\nu = \omega_k$ and $\nu t = p\pi$ for some $p \in \mathbb{N}$, we can write

$$r_{dc} = \operatorname{arcsinh}\left\{ ik\frac{A}{L_0}\frac{f_{\mathrm{RS}}^2(x_b)}{f_{\mathrm{RS}}(x_{t,0})}\left(\frac{1-(-1)^p}{3kf_{\mathrm{RS}}(x_b)} - \frac{\pi}{8}\frac{Ar_{\mathrm{S}}t}{L_0 x_{t,0}^2 f_{\mathrm{RS}}(x_{t,0})}\right)\right\}. \quad (5.52)$$

We may choose the encoded parameter to be $\epsilon = A/L_0$, for which the quantum Fisher information from equation 5.31 yields

$$H(\epsilon) = \frac{8\epsilon^2(C_1 - 2C_2\epsilon)^2(C_1 - C_2\epsilon)^2}{(1 - 2\epsilon^2(C_1 - C_2\epsilon)^2)^2}, \quad (5.53)$$

with

$$C_1 := \frac{f_{\mathrm{RS}}(x_b)}{f_{\mathrm{RS}}(x_{t,0})}\frac{1-(-1)^p}{3}$$
$$C_2 := \frac{f_{\mathrm{RS}}^2(x_b)}{f_{\mathrm{RS}}^2(x_{t,0})}\frac{k\pi r_{\mathrm{S}}t}{8x_{t,0}^2}.$$

We can see that C_2 is the relativistic correction, but it is 16 orders of magnitude smaller than C_1 for the parameters of our system.

Higher amplitudes improve the sensitivity, but there are limits on how big it can get. If we assume the 0.2 seconds interaction time again with the 2 mm/s speed of sound in the BEC, we get that $A \geq 40/(4p)\,\mu$m. The number of oscillations doesn't affect the sensitivities, as long as p is odd, therefore the most optimal case is when there is a single full oscillation with maximal amplitude. For $\mathcal{M} = 10^5$ measurements, we obtain the sensitivity to be $\Delta\epsilon = 0.02$ and relative sensitivity $\delta\epsilon = 0.14$.

In order to achieve higher sensitivities a displacement operator may be added to the measurement scheme. Employing the quantum frequency interferometre may improve sensitivities even further. There, the boundary motion would generate both single mode and two mode squeezing, each with their own squeezing parameter. As an interferometre, time dependent phonon frequencies would also enter the Fisher information, which would have an even more complicated form than before. One would also need to pay attention to using consistent coordinates throughout, compatible with the form of the Bogoliubov coefficients presented in [4].

Chapter 6

Conclusions

In this thesis we discussed and expanded on a novel way BECs could be used as an absolute gravimetre, first proposed in the patent [1]. We showed how quantum fields describing the phononic modes of a BEC can be quantised in the Schwarzschild metric, describing the curvature of spacetime around the Earth. The phonon frequency solutions of an elongated, vertically placed BEC were compared to a horizontally placed one. As only the vertical BEC couples to gravity, the horizontal BEC was used as reference. This replaces the need for an unrealistic point-like clock placed at infinity to be the reference for the frequencies. The patent mentions the possibility to do this but stops short from including it in its calculations.

The true novelty of the proposal lies in the interferometry scheme employed to estimate the effect of local gravitation. Current best interferometres, like the ones used for gravimetry, use spatial interferometry which have their sensitivities limited by the size of the interferometre arms and time of flight. On the other hand, quantum frequency interferometres promise to keep high precisions while keeping the system size small. This is achieved by carrying out the interferometry in the frequency domain using phonon modes trapped in a uniform box potential. To quantify the sensitivities, we used techniques from Gaussian quantum metrology and the covariance matrix formalism together with the quantum Cramér-Rao bound. We demonstrated the potential for enhancing the precision by harnessing quantum entanglement through a Gaussian unitary operation called the tritter, not considered in the patent. This improved sensitivities by 2 orders of magnitude.

Regrettably, the calculations presented in this thesis disagree with the calculations in the patent in several places. Some of these are believed to be

just potential minor typos in the patent and can be accounted for. However, there are discrepancies with severe consequences on the final results. One of these dissimilarities involves the expression for the gravity compensating potential, induced by a magnetic field gradient, given by 5.11. The patent presents a different expression, one that appears to have the wrong dimension for a potential energy. It is unclear to the author of this thesis how this expression was derived. Nonetheless, using the form of the potential given in this thesis an expression for the gravity induced density perturbation was derived (see equation 5.17) that is consistent with the patent. The issue appears again in the final expression for the relative error bound in estimating the Scwarzschild radius of the Earth. Following the derivation in the patent, in equation 5.46 the same expression was recovered for the relative error bound but with the difference of the inverse of the tuning parameter being replaced by the gravity compensating potential multiplied by the square of the radial distance from the centre of Earth. This causes issues with the dimensions again, as the relative error bound presented in the patent does not seem to be dimensionless neither by considering the previously obtained nor the expected dimensions for the external potential. On the contrary, the expression derived in this thesis for the relative error bound is shown to be dimensionless, as expected. It is possible that the symbol used in the patent is related to the tuning parameter in this final expression, rather than to the external potential.

However, these discrepancies discussed so far do not significantly impact the final results. The most critical difference is that the patent seems to neglect an assumption crucial for the derivation of the effective spacetime metric for the BEC, which believed to have profound consequences on the results found in this thesis. An overview of the derivation is given in section 3.2, with the full details found in [51]. This latter source also stresses that our description of phonons on a curved background is only possible if the relativistic quantum potential can be neglected. The authors then specify the necessary conditions for this, one of which is that the density of the BEC must vary slowly in space compared to the scales of the period of the phonons. This has a significant negative impact as the coupling of gravity to this density is precisely what our scheme uses to measure the effect of gravity. In equation 5.35 it is shown that the effect of gravity must be cancelled to an extreme precision for our theoretical model to remain valid. This limits the extent to which gravity can couple to our system and suppresses the sensitivities.

We plotted the sensitivities in the conventional units used for gravimetres for different values of the tuning parameter. The experimental parameters used in our calculations were based on actual reports from an experiment where a ^{87}Rb BEC was trapped in a box potential [68, 69], and a thorough analysis on BEC squeezing carried out by Paul Juschitz in his PhD thesis [72]. Inspecting the final expression for the relative error bound 5.2.2, it is clear that to lower its value one could attempt to increase the mode numbers, the interaction time, the length of the BEC, the tuning parameter, the number of particles in the BEC or the squeezing parameter. One must be careful however, as increasing some of these parameters may have undesirable effects. All of the listed parameters are limited by and depend strongly on the characteristics of the specific BEC that is prepared in the laboratory. The parameter values defined in this thesis are, to the best knowledge of the author, the most optimal for our purposes, which seem feasible with current technology. Future developments in BEC preparation could yield a setup that would result in improved sensitivities within our measurement scheme.

The state of the art commercial quantum technology measuring local gravity is from μQuans, reporting a sensitivity of 50 $\mu\text{Gal}/\sqrt{\text{Hz}}$ [78]. This is already a compact and portable device with an impressive precision, but even smaller, non-quantum devices are available on the market. For example, micro-electromechanical-system accelerometers can achieve sensitivities in the $\mu\text{Gal}/\sqrt{\text{Hz}}$ scales [79], while one such device capable of sensitivities in the sub-$\mu\text{Gal}/\sqrt{\text{Hz}}$ regime was landed on Mars by NASA's InSight mission [80]. Another BEC gravimetre has also been developed by a German group by preparing a BEC on a chip and letting it free-fall inside a cube of $1\,\text{cm}^3$ [66]. While this method differs from the one employed in this thesis, as it also uses the conventional spatial interferometry techniques, it still promises impressive sub-$\mu\text{Gal}/\sqrt{\text{Hz}}$ sensitivities. The competition is therefore fierce and the calculations of this thesis suggests that the gravimetre scheme being proposed must improve its sensitivities by at least 8 orders of magnitude before joining the race.

A potentially more fruitful use of the quantum frequency interferometry scheme could be to measure the effects of the dynamical Casimir effect. In section 5.2.3 we make the first steps towards this, following on from the work in [4]. We expect that the relativistic correction terms would also have a bigger impact on the sensitivities compared to a photonic system, due to the speed of sound in the BEC replacing the speed of light. It would be an interesting next step to employ the measurement scheme to this task and see what

precisions one might achieve. Of course, this experiment would still suffer from the need to cancel the gravitational force to an extremely high degree of precision in the vertical BEC for the phonons to stay alive. Nonetheless, we have presented some interesting use cases of the quantum frequency interferometre using a vertically oriented BEC, a tabletop experiment that could potentially be performed in a lab on the surface of Earth.

Bibliography

[1] Ivette Fuentes, Dennis Ratzel, Tupac Bravo Ibarra, and David Edward Bruschi. Quantum gravimeters and gradiometers, June 2 2022. US Patent App. 17/596,523.

[2] R. Howl and I. Fuentes. Quantum frequency interferometry: With applications ranging from gravitational wave detection to dark matter searches. *AVS Quantum Science*, 5(1), 01 2023. 014402.

[3] Tupac Bravo, Dennis Rätzel, and Ivette Fuentes. Gravitational time dilation in extended quantum systems: The case of light clocks in Schwarzschild spacetime. *AVS Quantum Science*, 5(1):014401, 01 2023.

[4] Maximilian P E Lock and Ivette Fuentes. Dynamical casimir effect in curved spacetime. *New Journal of Physics*, 19(7):073005, jul 2017.

[5] N. D. Birrell and P. C. W. Davies. *Quantum Fields in Curved Space*. Cambridge Monographs on Mathematical Physics. Cambridge University Press, 1982.

[6] Claus Kiefer. *Quantum Gravity*. Oxford University Press, 04 2012.

[7] Tobias Bothwell, Colin Kennedy, Alexander Aeppli, Dhruv Kedar, John Robinson, Eric Oelker, Alexander Staron, and Jun Ye. Resolving the gravitational redshift across a millimetre-scale atomic sample. *Nature*, 602:420, 2022-01 2022.

[8] Yanglin Hu, Maximilian P. E. Lock, and Mischa P. Woods. On the feasibility of detecting quantum delocalization effects on gravitational redshift in optical clocks, 2023.

[9] Shishir Khandelwal, Maximilian P.E. Lock, and Mischa P. Woods. Universal quantum modifications to general relativistic time dilation in delocalised clocks. *Quantum*, 4:309, August 2020.

[10] Carlos Sabín, David Edward Bruschi, Mehdi Ahmadi, and Ivette Fuentes. Phonon creation by gravitational waves. *New Journal of Physics*, 16(8):085003, aug 2014.

[11] Dennis Rätzel, Richard Howl, Joel Lindkvist, and Ivette Fuentes. Dynamical response of bose–einstein condensates to oscillating gravitational fields. *New Journal of Physics*, 20(7):073044, jul 2018.

[12] Steven Weinberg. *The Quantum Theory of Fields*. Cambridge University Press, 1995.

[13] V. Bargmann and E. P. Wigner. Group theoretical discussion of relativistic wave equations. *Proceedings of the National Academy of Sciences of the United States of America*, 34(5):211–223, 1948.

[14] Mark Srednicki. *Quantum Field Theory*. Cambridge University Press, 2007.

[15] N. N. Bogolyubov. On a New method in the theory of superconductivity. *Nuovo Cim.*, 7:794–805, 1958.

[16] Sean Carroll. *Spacetime and Geometry : an Introduction to General Relativity*. Pearson Education UK, 2013.

[17] Valerio Faraoni. *Special Relativity*. Springer Cham, 2013.

[18] W. Rindler. Kruskal Space and the Uniformly Accelerated Frame. *American Journal of Physics*, 34(12):1174–1178, 12 1966.

[19] L. Susskind and J. Lindesay. *An introduction to black holes, information and the string theory revolution: The holographic universe*. World Scientific Publishing Company, 2005.

[20] Michael Edward Peskin and Daniel V Schroeder. *An Introduction To Quantum Field Theory*. Westview Press, 1995.

[21] F. Halzen and A.D. Martin. *Quark & Leptons: an Introductory Course in Modern Particle Physics*. Wiley student edition. Wiley India Pvt. Limited, 2008.

[22] W. G. Unruh. Notes on black-hole evaporation. *Phys. Rev. D*, 14:870–892, Aug 1976.

[23] Shin Takagi. Vacuum Noise and Stress Induced by Uniform Acceleration: Hawking-Unruh Effect in Rindler Manifold of Arbitrary Dimension. *Progress of Theoretical Physics Supplement*, 88:1–142, 03 1986.

[24] Gerald T. Moore. Quantum Theory of the Electromagnetic Field in a Variable-Length One-Dimensional Cavity. *Journal of Mathematical Physics*, 11(9):2679–2691, 09 1970.

[25] C Wilson, G Johansson, A Pourkabirian, Michaël Simoen, Robert Johansson, Timothy Duty, Franco Nori, and P Delsing. Observation of the dynamical casimir effect in a superconducting circuit. *Nature*, 479:376–9, 11 2011.

[26] Leonard Parker and David Toms. *Quantum Field Theory in Curved Spacetime: Quantized Fields and Gravity*. Cambridge Monographs on Mathematical Physics. Cambridge University Press, 2009.

[27] Robert M. Wald. *Quantum Field Theory in Curved Space-Time and Black Hole Thermodynamics*. Chicago Lectures in Physics. University of Chicago Press, Chicago, IL, 1995.

[28] J. Dimock. Dirac quantum fields on a manifold. *Transactions of the American Mathematical Society*, 269:133–147, 1982.

[29] Roger Penrose. On gravity's role in quantum state reduction. *Gen. Rel. Grav.*, 28:581–600, 1996.

[30] Roger Penrose. On the Gravitization of Quantum Mechanics 1: Quantum State Reduction. *Found. Phys.*, 44:557–575, 2014.

[31] Dennis Rätzel, Fabienne Schneiter, Daniel Braun, Tupac Bravo, Richard Howl, Maximilian P E Lock, and Ivette Fuentes. Frequency spectrum of an optical resonator in a curved spacetime. *New Journal of Physics*, 20(5):053046, may 2018.

[32] Richard Howl, Roger Penrose, and Ivette Fuentes. Exploring the unification of quantum theory and general relativity with a bose–einstein condensate. *New Journal of Physics*, 21(4):043047, apr 2019.

[33] Hector A. Fernandez-Melendez, Alexander Belyaev, Vahe Gurzadyan, and Ivette Fuentes. Probing Lambda-Gravity with Bose-Einstein Condensate. 9 2024.

[34] Bose. Plancks gesetz und lichtquantenhypothese. *Zeitschrift für Physik*, 26:178–181, 1924.

[35] A. EINSTEIN. Quantentheorie des einatomigen idealen gases (zweite abhandlung). *S. B. Preuss. Akad. Wiss. phys-math. Klasse*, 13:3–14, 1925.

[36] Fritz London. The λ-phenomenon of liquid helium and the bose-einstein degeneracy. *Nature*, 141:643–644, 1938.

[37] N. N. Jr. Bogolyubov. On the theory of superfluidity. 1947.

[38] E P Gross. Structure of a quantized vortex in boson systems. *Nuovo Cimento (Italy) Divided into Nuovo Cimento A and Nuovo Cimento B*, 5 1961.

[39] P.P. Pitaevskii. Vortex lines in an imperfect bose gas. 13:451–454, 1961.

[40] Charles E Hecht. The possible superfluid behaviour of hydrogen atom gases and liquids. *Physica*, 25, 1959.

[41] K. Davis, Marc-Oliver Mewes, M. O, M. Andrews, Nicolaas Van Druten, Dallin Durfee, D. Kurn, and W. Ketterle. Bose-einstein condensation in a gas of sodium atoms. *Phys. Rev. Lett.*, 75:3969–, 11 1995.

[42] M. H. Anderson, J. R. Ensher, M. R. Matthews, C. E. Wieman, and E. A. Cornell. Observation of bose-einstein condensation in a dilute atomic vapor. *Science*, 269(5221):198–201, 1995.

[43] Curtis Bradley, Charles Sackett, J. Tollett, and R. Hulet. Evidence of bose-einstein condensation in an atomic gas with attractive interactions [phys. rev. lett. 75, 1687 (1995)]. *Physical review letters*, 75:1687–1690, 09 1995.

[44] Carlos Barceló, Stefano Liberati, and Matt Visser. Analogue gravity. *Living Reviews in Relativity*, 8, 2005.

[45] L. J. Garay, J. R. Anglin, J. I. Cirac, and P. Zoller. Sonic analog of gravitational black holes in bose-einstein condensates. *Physical Review Letters*, 85(22):4643–4647, November 2000.

[46] L. J. Garay, J. R. Anglin, J. I. Cirac, and P. Zoller. Sonic black holes in dilute bose-einstein condensates. *Physical Review A*, 63(2), January 2001.

[47] W. G. Unruh. Experimental black-hole evaporation? *Phys. Rev. Lett.*, 46:1351–1353, May 1981.

[48] Oren Lahav, Amir Itah, Alex Blumkin, Carmit Gordon, Shahar Rinott, Alona Zayats, and Jeff Steinhauer. Realization of a sonic black hole analog in a bose-einstein condensate. *Physical Review Letters*, 105(24), December 2010.

[49] C. J. Pethick and H. Smith. *Bose–Einstein Condensation in Dilute Gases*. Cambridge University Press, 2 edition, 2008.

[50] Lev Pitaevskii and Sandro Stringari. *Bose-Einstein Condensation and Superfluidity*. Oxford University Press, 01 2016.

[51] S Fagnocchi, S Finazzi, S Liberati, M Kormos, and A Trombettoni. Relativistic bose–einstein condensates: a new system for analogue models of gravity. *New Journal of Physics*, 12(9):095012, September 2010.

[52] Matt Visser and Carmen Molina-París. Acoustic geometry for general relativistic barotropic irrotational fluid flow. *New Journal of Physics*, 12(9):095014, sep 2010.

[53] Dominik Šafránek. Gaussian quantum metrology and space-time probes, December 2016.

[54] Ulrik L Andersen, Tobias Gehring, Christoph Marquardt, and Gerd Leuchs. 30 years of squeezed light generation. *Physica Scripta*, 91(5):053001, apr 2016.

[55] Rafał Demkowicz-Dobrzański, Konrad Banaszek, and Roman Schnabel. Fundamental quantum interferometry bound for the squeezed-light-enhanced gravitational wave detector geo 600. *Phys. Rev. A*, 88:041802, Oct 2013.

[56] Akira Furusawa and Nobuyuki Takei. Quantum teleportation for continuous variables and related quantum information processing. *Physics Reports-review Section of Physics Letters - PHYS REP-REV SECT PHYS LETT*, 443:97–119, 05 2007.

[57] E. L. Lehmann and George Casella. *Theory of Point Estimation*. 1998.

[58] S. Amari and H. Nagaoka. *Methods of Information Geometry*. Translations of mathematical monographs. American Mathematical Society, 2000.

[59] Pieter Kok and Brendon W. Lovett. *Introduction to Optical Quantum Information Processing*. 2010.

[60] MATTEO G. A. PARIS. Quantum estimation for quantum technology. *International Journal of Quantum Information*, 07(supp01):125–137, 2009.

[61] A. Uhlmann. The "transition probability" in the state space of a -algebra. *Reports on Mathematical Physics*, 9(2):273–279, 1976.

[62] Alessandro Ferraro, Stefano Olivares, and Matteo G. A. Paris. Gaussian states in continuous variable quantum information, 2005.

[63] Christian Weedbrook, Stefano Pirandola, Raú l García-Patrón, Nicolas J. Cerf, Timothy C. Ralph, Jeffrey H. Shapiro, and Seth Lloyd. Gaussian quantum information. *Reviews of Modern Physics*, 84(2):621–669, may 2012.

[64] Dominik Šafránek, Antony R. Lee, and Ivette Fuentes. Quantum parameter estimation using multi-mode Gaussian states. *New Journal of Physics*, 17(7):073016, July 2015.

[65] Dominik Šafránek. Simple expression for the quantum fisher information matrix. *Physical Review A*, 97, 01 2018.

[66] Sven Abend. *Atom-chip gravimeter with Bose-Einstein condensates*. PhD thesis, Leibniz U., Hannover, 2017.

[67] Stuart S. Szigeti, Samuel P. Nolan, John D. Close, and Simon A. Haine. High-precision quantum-enhanced gravimetry with a bose-einstein condensate. *Physical Review Letters*, 125(10), September 2020.

[68] Alexander L. Gaunt, Tobias F. Schmidutz, Igor Gotlibovych, Robert P. Smith, and Zoran Hadzibabic. Bose-einstein condensation of atoms in a uniform potential. *Phys. Rev. Lett.*, 110:200406, May 2013.

[69] Igor Gotlibovych, Tobias F. Schmidutz, Stuart Moulder, Robert L. D. Campbell, Naaman Tammuz, Richard J. Fletcher, Alexander L. Gaunt, Scott Beattie, Robert P. Smith, and Zoran Hadzibabic. A compact single-chamber apparatus for bose-einstein condensation of ^{8}7rb, 2012.

[70] Carl W Helstrom. *Quantum detection and estimation theory*. New York: Academic Press, 1976.

[71] Carlos Sabín, Jan Kohlrus, David Bruschi, and Ivette Fuentes. Thermal noise in bec-phononic gravitational wave detectors. *EPJ Quantum Technology*, 3, 05 2015.

[72] Paul Juschitz. Two-mode phonon squeezing in bose-einstein condensates for gravitational wave detection, 2021.

[73] Roman Schnabel. Squeezed states of light and their applications in laser interferometers. *Physics Reports*, 684:1–51, 2017. Squeezed states of light and their applications in laser interferometers.

[74] C. Gross, T. Zibold, E. Nicklas, J. Estève, and M. K. Oberthaler. Nonlinear atom interferometer surpasses classical precision limit. *Nature*, 464(7292):1165–1169, March 2010.

[75] J. Estève, C. Gross, A. Weller, S. Giovanazzi, and M. K. Oberthaler. Squeezing and entanglement in a bose–einstein condensate. *Nature*, 455(7217):1216–1219, October 2008.

[76] W. Muessel, H. Strobel, D. Linnemann, T. Zibold, B. Juliá-Díaz, and M. K. Oberthaler. Twist-and-turn spin squeezing in bose-einstein condensates. *Phys. Rev. A*, 92:023603, Aug 2015.

[77] Lin Xin, Maryrose Barrios, Julia T. Cohen, and Michael S. Chapman. Long-lived squeezed ground states in a quantum spin ensemble. *Phys. Rev. Lett.*, 131:133402, Sep 2023.

[78] $\mu Quans.https://www.muquans.com/.Accessed: 21-11-2024.$

[79] Shihao Tang, Huafeng Liu, Shitao Yan, Xiaochao Xu, Wenjie Wu, Ji Fan, Jinquan Liu, Chenyuan Hu, and Liang Cheng Tu. A high-sensitivity mems gravimeter with a large dynamic range. *Microsystems & Nanoengineering*, 5, 2019.

[80] William Thomas Pike, Ian M. Standley, Simon Calcutt, and A. G. Mukherjee. A broad-band silicon microseismometer with 0.25 ng/rthz performance. *2018 IEEE Micro Electro Mechanical Systems (MEMS)*, pages 113–116, 2018.

Appendix A

Bogoliubov coefficients

First, we note that we may choose the point of transition where the field inside the box goes from being inertial to non-inertial be at $t = 0$. At this point $\zeta = 0$ and $\chi = x$. This allows us to write down the inner product as

$$\begin{aligned}\alpha_{mn} &= -i \int_{\Sigma} dx \big(\phi_n^M \frac{1}{\chi} \partial^{\zeta} \phi_m^{R*} - \phi_m^{R*} \partial^t \phi_n^M 0\big) \\ &= \int_{x_l}^{x_r} dx \frac{1}{\sqrt{\omega_n \Omega_m L \ln \frac{x_r}{x_l}}} \left(\omega_n + \frac{\Omega_m}{x}\right) \sin\big(\omega_n (x - x_l)\big) \sin\big(\Omega_m \ln \frac{x}{x_l}\big).\end{aligned} \tag{A.1}$$

This integral has no analytical solutions, however, we can find an approximation by introducing the dimensionless parameter h defined as

$$h := \frac{\alpha_c L}{c^2} = \frac{L}{\chi_c}. \tag{A.2}$$

Note that for all practical cases $\alpha_c L \ll c^2$, which in turn means that $h \ll 1$. We can utilise this to rewrite the integrand in terms of h and then Taylor expand around $h = 0$. Using the expressions $\alpha_c = \frac{2c^2}{\chi_l + \chi_r}$ and $L = \chi_r - \chi_l$ we can write $\chi_{l,r}$ in terms of h:

$$\begin{aligned}\chi_l &= \left(\frac{1}{h} - \frac{1}{2}\right) L \\ \chi_r &= \left(\frac{1}{h} + \frac{1}{2}\right) L\end{aligned} \tag{A.3}$$

We may plug this into $\ln \frac{\chi_r}{\chi_l}$ and note using an identity that

$$\ln \frac{\chi_r}{\chi_l} = \ln \left(\frac{1 + \frac{h}{2}}{1 - \frac{h}{2}} \right) = 2 \tanh^{-1} \left(\frac{h}{2} \right), \tag{A.4}$$

which holds for $\frac{h}{2} < 1$. Before the series expansion, we first also perform a change of variables. We define a new variable as

$$x' := x + x_l. \tag{A.5}$$

The new limits after the substitution are 0 and L. The integral now has the form

$$\int_0^L dx' \frac{1}{\sqrt{mn}} \left(\frac{n}{L} + \frac{m}{2 \tanh^{-1} \left(\frac{h}{2} \right) (x_l + x')} \right) \sin \left(\frac{\pi n x'}{L} \right) \sin \left(\frac{\pi m \ln \left(\frac{x'}{x_l} + 1 \right)}{2 \tanh^{-1} \left(\frac{h}{2} \right)} \right) \tag{A.6}$$

Taylor expanding around $h = 0$ gives

$$\int_0^L dx' \left[\frac{(m+n) \sin \left(\frac{\pi n x'}{L} \right) \sin \left(\frac{\pi m x'}{L} \right)}{L \sqrt{mn}} + \right.$$
$$\left. + \frac{\sin \left(\frac{\pi n x'}{L} \right) \left(\frac{\pi m \left(L x' - x'^2 \right) (m+n) \sin' \left(\frac{\pi m x'}{L} \right)}{2L^3} + \frac{m(L - 2x') \sin \left(\frac{\pi m x'}{L} \right)}{2L^2} \right)}{\sqrt{mn}} h + \mathcal{O}\left(h^2\right) \right]. \tag{A.7}$$

The integral can now be evaluated to obtain the α-type coefficients, and similarly the β-type coefficients.

Appendix B

The real and complex representations

The position and momentum operators are related to the field mode operators via

$$\begin{aligned} \hat{x}_n :=& \frac{1}{\sqrt{2}} \left(\hat{a}_n + \hat{a}_n^\dagger \right) \\ \hat{p}_n :=& \frac{-i}{\sqrt{2}} \left(\hat{a}_n - \hat{a}_n^\dagger \right) . \end{aligned} \tag{B.1}$$

We may collect $2N$ of these bosonic operators into vectors

$$\hat{\mathbf{Q}} = \begin{bmatrix} \hat{x}_1 \\ \vdots \\ \hat{x}_N \\ \hat{p}_1 \\ \vdots \\ \hat{p}_N \end{bmatrix} , \hat{\mathbf{A}} \;\; = \begin{bmatrix} \hat{a}_1 \\ \vdots \\ \hat{a}_N \\ \hat{a}_1^\dagger \\ \vdots \\ \hat{a}_N^\dagger \end{bmatrix} . \tag{B.2}$$

Vector $\hat{\mathbf{Q}}$ defines the *real representation* and $\hat{\mathbf{A}}$ the *complex representation*. We define the transformation matrix between the two representations as $\hat{\mathbf{A}} = \mathbf{U}\hat{\mathbf{Q}}$, where

$$\mathbf{U} = \frac{1}{\sqrt{2}} \begin{bmatrix} \mathbf{I}_{N\times N} & i\mathbf{I}_{N\times N} \\ \mathbf{I}_{N\times N} & -i\mathbf{I}_{N\times N} \end{bmatrix} , \tag{B.3}$$

with $\mathbf{I}_{N\times N}$ the $N \times N$ dimensional identity matrix. Unfortunately, these are not the only two forms used in the literature, but sometimes authors reorder

these vectors as

$$\tilde{\hat{\mathbf{Q}}} = \begin{bmatrix} \hat{x}_1 \\ \hat{p}_1 \\ \vdots \\ \hat{x}_N \\ \hat{p}_N \end{bmatrix}, \tilde{\hat{\mathbf{A}}} = \begin{bmatrix} \hat{a}_1 \\ \hat{a}_1^\dagger \\ \vdots \\ \hat{a}_N \\ \hat{a}_N^\dagger \end{bmatrix}. \tag{B.4}$$

It is easy to swap between representations using the basis changing matrix $\mathbf{L}$:

$$\begin{aligned} \tilde{\hat{\mathbf{Q}}} &= \mathbf{L}\hat{\mathbf{Q}} \\ \tilde{\hat{\mathbf{A}}} &= \mathbf{L}\hat{\mathbf{A}}, \end{aligned} \tag{B.5}$$

where the non-zero matrix elements are $L_{(2k-1,k)} = L_{(2k,N+k)} = 1$ with $k \in [1, N]$. In addition, we define the transformation matrix in this representation as $\tilde{\hat{\mathbf{A}}} = \tilde{\mathbf{U}}\tilde{\hat{\mathbf{Q}}}$, where

$$\tilde{\mathbf{U}} = \mathbf{L}\mathbf{U}\mathbf{L}^{-1} = \frac{1}{\sqrt{2}} \begin{bmatrix} \mathbf{u} & \mathbf{0} & \dots & \mathbf{0} \\ \mathbf{0} & \mathbf{u} & \dots & \mathbf{0} \\ \vdots & \ddots & \ddots & \vdots \\ \mathbf{0} & \dots & \mathbf{0} & \mathbf{u} \end{bmatrix}, \tag{B.6}$$

where $\mathbf{0}$ is the 2×2 zero matrix and

$$\mathbf{u} = \begin{bmatrix} 1 & i \\ 1 & -i \end{bmatrix}. \tag{B.7}$$

We also note that in this basis representation the equivalent symplectic form is $\tilde{K} = diag(1, -1, ..., 1, -1)$.